1
Theory of dipolar gases

In these notes I discuss some interesting features of the physics of dipolar gases, with a particular emphasis on those phenomena which differ qualitatively from those known in non-dipolar gases. These notes do not intend to be a complete review on previous work on dipolar gases (for that see recent reviews (Baranov, 2008; Lahaye *et al.*, 2009)), and in this sense I apologise from the very beginning to those whose work is not explicitly cited here. I have tried to condense as much as possible adapting to the reduced time of three lectures, and this has forced me to leave some very interesting topics aside, including most of the theory of dipolar Fermi gases, crystallisation and rapidly-rotating dipolar gases. I apologise for that. I hope that these notes will serve however as a basic introduction to the topic of dipolar gases, and in particular of why dipolar gases are so interesting, since indeed dipolar gases (most relevantly polar molecules) may change the rules of the game!

1.1 The dipole-dipole interaction

Before discussing the physics of dipolar gases, it is of crucial importance to understand the main features of the dipole-dipole interaction (DDI). We shall have a look as well to various examples of dipolar gases.

1.1.1 Main features of the dipole-dipole interaction

For two particles with dipole moments along the unit vectors $\boldsymbol{e}_1$ and $\boldsymbol{e}_2$, and whose relative position is $\boldsymbol{r}$ (see Fig. 1.1), the energy due to the DDI reads

$$U_{\rm dd}(\boldsymbol{r}) = \frac{C_{\rm dd}}{4\pi}\frac{(\boldsymbol{e}_1\cdot\boldsymbol{e}_2)\,r^2 - 3\,(\boldsymbol{e}_1\cdot\boldsymbol{r})\,(\boldsymbol{e}_2\cdot\boldsymbol{r})}{r^5}. \tag{1.1}$$

The coupling constant $C_{\rm dd}$ is $\mu_0\mu^2$ for particles having a permanent magnetic dipole moment μ (μ_0 is the permeability of vacuum) and d^2/ε_0 for particles having a permanent electric dipole moment d (ε_0 is the permitivity of vacuum). For a polarised sample where all dipoles point in the same direction z (Fig. 1.1b), this expression simplifies to

$$U_{\rm dd}(\boldsymbol{r}) = \frac{C_{\rm dd}}{4\pi}\frac{1-3\cos^2\theta}{r^3}, \tag{1.2}$$

where θ is the angle between the direction of polarisation and the relative position of the particles.

This interaction must be compared with the (up to now) usual van-der-Waals-like interaction $-C_6/r^6$, which is both isotropic and short-range. On the contrary the DDI is:

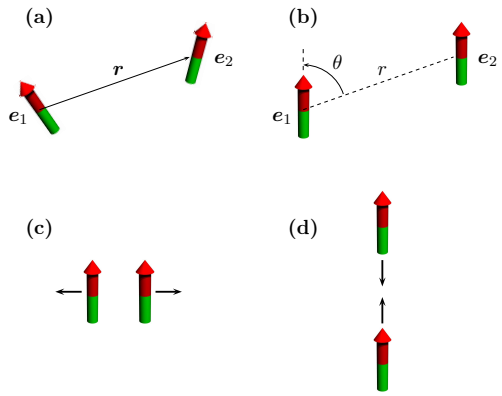

Fig. 1.1 Two particles interacting via the dipole-dipole interaction. (a) Non-polarised case; (b) Polarised case; (c) Two polarised dipoles side by side repel each other (black arrows); (d) Two polarised dipoles in a 'head to tail' configuration attract each other (black arrows).

- Anisotropic. As θ varies between 0 and $\pi/2$, the factor $1-3\cos^2\theta$ varies between -2 and 1, and thus the DDI is repulsive for particles sitting side by side, while it is attractive for dipoles in a 'head-to-tail' configuration (see Fig. 1.1(c) and (d)). For the special value $\theta_{\mathrm{m}} = \arccos\left(1/\sqrt{3}\right) \simeq 54.7°$ ('magic-angle') the DDI vanishes.
- Long-range. One must recall that in a 3D scattering, a potential $U(\boldsymbol{r})$ is long-range if it decays as $1/r^n$ with $n \leq 3$. In that case $\int U(\boldsymbol{r})\,\mathrm{d}^3 r$ diverges. In this sense, the DDI is strictly long-range in three dimensions.

1.1.2 Scattering properties. Pseudo-potential

The long-range anisotropic character of the DDI leads to peculiar low-energy scattering properties: not only the s-wave, but all partial waves contribute to scattering, in contrast to the case of a short-range interaction, where only s-wave scattering typically matters. Here we should recall the general theory of low-energy scattering (see, e.g. Ref. (Landau and Lishitz, 1977)), which states that for a central potential falling off at large distances like $1/r^n$, the scattering phase shifts $\delta_\ell(k)$ scale, for $k \to 0$, like $k^{2\ell+1}$ if $\ell < (n-3)/2$, and like k^{n-2} otherwise (Landau and Lishitz, 1977). For a van der Waals-like potential ($n = 6$), only $l = 0$ (s-wave) matters at low energies. In the ultracold regime, the scattering is thus fully characterised by the s-wave scattering length a. In the study of quantum gases, the true short-range interaction potential between the atoms can then be replaced by a pseudo-potential having the same scattering length, the so-called contact interaction, given by $4\pi\hbar^2 a\delta(\boldsymbol{r})/m \equiv g\delta(\boldsymbol{r})$.

The situation is very different if in addition to the short-range interactions there is a significant DDI. The $1/r^3$ decay at large distances implies that for all ℓ, $\delta_\ell \sim k$ at low momentum, and all partial waves contribute to the scattering amplitude. Moreover, due to the anisotropy of the DDI, the angular momentum (i.e. l) is not conserved during scattering, and as a consequence the DDI mixes all partial waves with even (for the case of bosons) and odd (for the case of fermions) angular momenta. For dipoles

polarised along z, cylindrical symmetry is however preserved and the m quantum number (related to the projection L_z of the angular momentum) is hence preserved. The scattering matrix is hence of the form $t_{l,m}^{l',m'} = t_l^{l'}\delta_{m,m'}$, where (l,m) and (l',m') characterise the incoming and outgoing channels, respectively. The problem may be rigorously treated by means of a multi-channel scattering theory, but we will not discuss all details here (see e.g. (Marinescu and You, 1998)). The main conclusions of this theory is that we may substitute the actual inter-particle interaction by an effective pseudo-potential of the simple form:

$$U(\boldsymbol{r}) = g\delta(\boldsymbol{r}) + U_{dd}(\boldsymbol{r}), \tag{1.3}$$

where g is defined as above, but in principle $a = a(d)$. Note that due to coupling between different scattering channels, the DDI generates a short-range contribution to the total effective potential in the s-wave channel (l = 0) that adds to the short-range part of the inter-particle interaction. As a result, by changing the strength of the DDI one may modify a as well. This may manifest itself quite dramatically in the appearance of scattering resonances, so-called shape resonances (see e.g.(Marinescu and You, 1998; Deb and You, 2001; Bortolotti *et al.*, 2006)), when a virtual state transforms into a new bound state. The previous pseudo-potential has been shown to be valid away from shape resonances (Deb and You, 2001; Bortolotti *et al.*, 2006).

The scattering of bosonic dipoles is hence determined by both long-range and short-range interactions, whose interplay plays, as we shall see, a crucial role in the physics of dipolar BECs. For fermionic dipoles the s-wave channel is absent, and hence the low-energy scattering of fermionic dipoles is determined only by the long-range part. This is of course crucial for polarised Fermi gases, since contrary to the case of a short-range interaction, which freezes out at low temperature, the collisional cross section for identical fermions interacting via the DDI does not vanish even at zero temperature.

1.1.3 Fourier transform of the dipole-dipole interaction

In the analysis of dipolar gases, the Fourier transform of the DDI turns out to be very helpful. This Fourier transform may be easily retrieved by re-writing:

$$U_{dd}(\boldsymbol{r}) = \frac{C_{dd}}{4\pi r^3}\left(-4\sqrt{\frac{\pi}{5}}\right)Y_{20}(\theta), \tag{1.4}$$

where Y_{lm} are the spherical harmonics. We employ the expansion of a plane wave in spherical harmonics:

$$e^{-i\boldsymbol{k}\cdot\boldsymbol{r}} = 4\pi\sum_{l=0}^{\infty} i^l j_l(kr)\sum_{m=-l}^{l} Y_{lm}^*(\theta,\phi)Y_{lm}(\theta_k,\phi_k). \tag{1.5}$$

Employing the orthonormality of the spherical harmonics $\int d\theta \sin\theta d\phi Y_{lm}^* Y_{l',m'} = \delta_{ll'}\delta_{mm'}$, and $\int dr j_2(kr)/r = 1/3$, we may then easily obtain that

$$\tilde{U}_{dd}(\boldsymbol{k}) = \int d^3r U_{dd}(\boldsymbol{r})e^{-i\boldsymbol{k}\cdot\boldsymbol{r}} = \frac{C_{dd}}{3}\left(3\cos^2\theta_k - 1\right). \tag{1.6}$$

This must be compared to the short-range interaction, which due to its contact character presents no momentum dependence. This different momentum dependence of

both interactions plays a crucial role in the physics of dipolar gases, and more so in the presence of trapping, as we shall see later on in these notes.

1.1.4 Dipolar gases: from tiny to huge dipoles

Before entering into the detailed discussion of dipolar gases, we should discuss what do we actually mean by a dipolar gas. A gas may be defined as dipolar if the DDI plays at least some role in its properties. This of course is a very broad definition, which may include from tiny to huge dipoles, since whether the DDI is important or not largely depends on other energy scales.

As mentioned above, the interplay between DDI and short-range interactions is crucial in dipolar gases. We may quantify this interplay by the ratio

$$\epsilon_{dd} = C_{dd}/3g \tag{1.7}$$

between the dipole strength (given by the prefactor $C_{dd}/3$ of $\tilde{U}_{dd}$) and the short-range coupling constant g. In principle a dominant DDI demands $\epsilon_{dd} > 1$, although dipolar effects may occur even for $\epsilon_{dd} \ll 1$, as we discuss below.

In the following, we discuss some interesting details concerning atomic magnetic dipoles and polar molecules, skipping the discussion about e.g. Rydberg gases, which may present an extraordinarily large dipole moment, although a short life time as well.

Atomic magnetic dipoles. In alkali atoms, the maximum magnetic moment in the ground state is $\mu = 1\mu_B$ (with μ_B the Bohr magneton), and thus the magnetic dipolar effects are very weak. However, reducing the scattering length to $a \simeq 0$ by means of magnetic fields (Feshbach resonances) may allow to observe effects of the magnetic DDI (Fattori *et al.*, 2008; Pollack *et al.*, 2009). However, this is not even necessary, because ϵ_{dd} do not always fully characterise the importance of the DDI. This is particularly the case of spinor gases, which are composed by various internal Zeeman states. Spin-changing collisions, which are crucial in the magnetic properties of these gases, are typically characterised by a very low energy. As a result, even a weak DDI, as that of e.g. ^{87}Rb F=1, may lead to a strong modification of the magnetic properties of spinor condensates, as recently observed at Berkeley (Vengalattore *et al.*, 2008).

Some other atoms, like Chromium, Erbium, Europium, Dysprosium, and others, have a large magnetic moment of several μ_B in their ground state, and thus experience significant magnetic DDI. Among them, only Chromium has been Bose-condensed to date (Griesmaier *et al.*, 2005; Beaufils *et al.*, 2008). Chromium has a magnetic dipole moment of $6\,\mu_{\mathrm{B}}$, and a scattering length of about $100\,a_0$ (Schmidt *et al.*, 2003). This gives $\varepsilon_{\mathrm{dd}} \simeq 0.16$ (Griesmaier *et al.*, 2006), which allows to observe a perturbative effect of the dipolar interaction on the expansion dynamics of the cloud (Stuhler *et al.*, 2005). The role of the DDI may be enhanced by means of Feshbach resonances as shown in recent experiments in Stuttgart (Lahaye *et al.*, 2008).

Polar molecules. Polar molecules constitute a huge leap in dipole moment (this time electric). Heteronuclear molecules as KRb may present dipole moments larger than 0.5 Debye ($1\,\mathrm{D} \simeq 3.335 \times 10^{-30}\,\mathrm{C}\cdot\mathrm{m}$). This must be compared to Chromium, which has a dipole moment equivalent to 0.05 D. Recall that the DDI is proportional to d^2, and hence polar molecules may present a DDI two orders of magnitude (or even more)

than Chromium. Dipolar effects are hence expected to be dominant in quantum gases of polar molecules ($\epsilon_{dd} \simeq 20$ for fully polarised KRb).

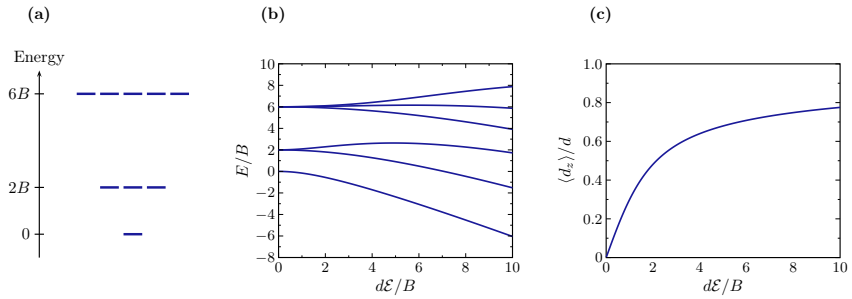

Fig. 1.2 (a) Rotational spectrum of a diatomic molecule in zero field. (b) Dependence of the first energy levels on the applied electric field $\mathcal{E}$. (c) the ground state average dipole moment $\langle d_z \rangle$ in the laboratory frame as a function of the applied field $\mathcal{E}$. Figure from Ref. (Lahaye *et al.*, 2009).

A polar molecule is maximally polar when placed into its lowest ro-vibrational state (the dipole moment scales asymptotically as R^{-7} with the inter-nuclear separation R (Kotochigova *et al.*, 2003)). However, although a molecule may exhibit a permanent dipole moment $\hat{\boldsymbol{d}}$ in the molecular frame, it must be oriented in the laboratory frame by an external electric field.

This orientation may be understood from a rigid rotor ("dumb-bell") model which is a simple model of diatomic molecules, which are considered basically two atoms joined by a rigid (weightless) rod. The Hamiltonian for a rigid rotor reads $\hat{H}_{\rm rot} = B\hat{\boldsymbol{J}}^2$ where $\hat{\boldsymbol{J}}$ is the molecule angular momentum operator (in units of $\hbar$) and B the rotational constant, linked to the equilibrium inter-nuclear distance R and the reduced mass $m_{\rm r}$ by the relationship $B = \hbar^2/(2m_{\rm r}R^2)$; its typical order of magnitude is $B/h \sim 10$ GHz. The eigenstates of $\hat{H}_{\rm rot}$ (i.e. the rotational spectrum) are the angular momentum eigenstates $|J, m_J\rangle$ with energy $BJ(J+1)$, and are $2J+1$ times degenerate (Fig. 1.2(a)).

This degeneracy is lift in the presence of an external field $\boldsymbol{E} = \mathcal{E}\boldsymbol{e}_z$, which leads to a Stark shift $\hat{H} = \hat{H}_{\rm rot} - d\mathcal{E}\cos\theta$, with θ the angle between z and the inter-nuclear axis (Fig. 1.2(b)). We may then obtain the average dipole moment $\langle d_z \rangle = d\langle\cos\theta\rangle$ for the ground state using the Hellmann-Feynman theorem: $\langle d_z \rangle = -\frac{\partial E_0}{\partial \mathcal{E}}$, where $E_0(\mathcal{E})$ is the ground state energy. The dipole moment $\langle d_z \rangle$ increases linearly at small $\mathcal{E}$, saturating asymptotically for $d\mathcal{E} \gg B$ towards a value d (Fig. 1.2(c)). For typical values $d \sim 1$ D and $B/h \sim 10$ GHz, the electric field strength corresponding to $d\mathcal{E} \sim B$ is on the order of 10^4 V/cm, which, from the experimental point of view, is accessible in a relatively easy way. Note finally, that $B \sim m_r^{-1}$ and smaller m_r means larger B and hence larger $\mathcal{E}$ to polarise (e.g. LiCs is more difficult to orient than KRb). For more details on the orientation of polar molecules, see e.g. (Micheli *et al.*, 2007).

As for this moment, polar molecules have not been yet brought to quantum degeneracy, but this quest constitutes nowadays the focus of very active on-going efforts.

Interestingly, polar molecules in the lowest ro-vibrational and hyperfine states have been recently achieved (Ni *et al.*, 2008; Deiglmayr *et al.*, 2008). I will not comment in detail about that since a lecture was provided on this topic was provided in the Les Houches school by D. Jin.

1.2 Dipolar Bose-Einstein condensates

We shall have a look now to the properties of dipolar bosons, and in particular of dipolar BECs (more extensive reviews may be found in Refs. (Baranov, 2008; Lahaye *et al.*, 2009)). We shall focus on relatively simple scenarios, discussing some key features including the different forms of instability, and some interesting non-linear phenomena in dipolar BECs.

1.2.1 Non-local Gross-Pitaevskii equation

Let us consider a gas of dipolar bosons. The second-quantized Hamiltonian of the system reads:

$$\hat{H} = \int d\boldsymbol{r}\hat{\psi}^\dagger(\boldsymbol{r})\left[-\frac{\hbar^2}{2m}\nabla^2 + V(\boldsymbol{r}) - \mu\right]\hat{\psi}(\boldsymbol{r}) + \frac{1}{2}\int d\boldsymbol{r}d\boldsymbol{r}'\hat{\psi}^\dagger(\boldsymbol{r})\hat{\psi}^\dagger(\boldsymbol{r}')U(\boldsymbol{r}-\boldsymbol{r}')\hat{\psi}(\boldsymbol{r}')\hat{\psi}(\boldsymbol{r}), \tag{1.8}$$

where $\hat{\psi}(\boldsymbol{r})$ and $\hat{\psi}^\dagger(\boldsymbol{r})$ are the particle annihilation and creation operators, which fulfil the usual bosonic commutation relations, $V(\boldsymbol{r})$ is the trapping potential, and μ is the chemical potential. The interaction potential $U(\boldsymbol{r})$ may be approximated by the pseudo-potential (1.3), and then our Hamiltonian becomes:

$$\hat{H} = \int d\boldsymbol{r}\hat{\psi}^\dagger(\boldsymbol{r})\left[-\frac{\hbar^2}{2m}\nabla^2 + V(\boldsymbol{r}) - \mu + \frac{1}{2}g\hat{\psi}^\dagger(\boldsymbol{r})\hat{\psi}(\boldsymbol{r})\right]\hat{\psi}(\boldsymbol{r}) + \frac{1}{2}\int d\boldsymbol{r}d\boldsymbol{r}'\hat{\psi}^\dagger(\boldsymbol{r})\hat{\psi}^\dagger(\boldsymbol{r}')U_{dd}(\boldsymbol{r}-\boldsymbol{r}')\hat{\psi}(\boldsymbol{r}')\hat{\psi}(\boldsymbol{r}), \tag{1.9}$$

We may then obtain easily the Heisenberg equations for the dynamics of the field operators, by employing the bosonic commutation rules. Since we are interested in the case of BECs far from the critical condensation temperature, we may introduce the usual Bogoliubov approximation $\hat{\psi}(\boldsymbol{r}) \simeq \psi(\boldsymbol{r})$. In this way we obtain that the Heisenberg equation transforms into the following equation for the dynamics of the condensate wavefunction:

$$i\hbar\frac{\partial}{\partial t}\psi(\boldsymbol{r},t) = \left[-\frac{\hbar^2}{2m}\nabla^2 + V(\boldsymbol{r}) - \mu + g|\psi(\boldsymbol{r},t)|^2 + \frac{C_{dd}}{4\pi}\int d\boldsymbol{r}'\frac{1-3\cos^2\theta}{|\boldsymbol{r}-\boldsymbol{r}'|^3}|\psi(\boldsymbol{r}',t)|^2\right]\psi(\boldsymbol{r},t). \tag{1.10}$$

Note that this equation is a modified version of the well-known Gross-Pitaevskii equation (GPE), or equivalently the non-linear Schrödinger equation. In the absence

of DDI the nonlinearity is given by the term $g|\psi(\boldsymbol{r})|^2$ term, an hence it is a local nonlinearity similar to that found in many Kerr media in nonlinear optics. On the contrary the nonlinearity introduced by the DDI is non-local, i.e. the wavefunction in $\boldsymbol{r}$ depends on the wavefunction in $\boldsymbol{r}'$ through a kernel given by $U_{dd}(\boldsymbol{r}-\boldsymbol{r}')$. Interestingly, this links the physics of dipolar BECs with other non-local nonlinear systems, as e.g. plasmas where the non-locality is introduced by thermal effects (Litvak *et al.*, 1975), or nematic liquid crystals (Conti *et al.*, 2003), where the non-local nonlinearity is given by long-range inter-molecular interactions.

1.2.2 Phonon instability

The DDI is attractive along some directions, and repulsive along some others. In some sense, we should hence naively expect a sort of hybrid behaviour between a repulsive gas (as that of a non-dipolar gas with $a > 0$) and an attractive gas (as that of a non-dipolar gas with $a < 0$). Interestingly, this is to some extent what happens. In particular, we know that a gas with attractive interactions has a dangerous tendency to collapse.

Stability is hence an issue of obvious concern in dipolar gases. Let us try to understand this important point in more detail. We shall consider a simplified 3D homogeneous model (no trapping), and perform a standard Bogoliubov-de Gennes analysis of the stability. We consider a 3D BEC with a density n_0. Is the dipolar BEC stable? We shall quickly see that the answer may be no!

Let us return to the Hamiltonian (1.8). We introduce the Fourier transform $\hat{\psi}(\boldsymbol{r}) = \sum_{\boldsymbol{p}} \hat{a}_{\boldsymbol{p}} \exp[i\boldsymbol{p}\cdot\boldsymbol{r}/\hbar]\sqrt{V}$, where V is a quantisation volume. This leads to the Hamiltonian in momentum space:

$$\hat{H} = \sum_{\boldsymbol{p}} \frac{p^2}{2m} \hat{a}^\dagger_{\boldsymbol{p}} \hat{a}_{\boldsymbol{p}} + \frac{1}{2V} \sum_{\boldsymbol{p}_1,\boldsymbol{p}_2,\boldsymbol{q}} \tilde{U}(\boldsymbol{q}) \hat{a}^\dagger_{\boldsymbol{p}_1+\boldsymbol{q}} \hat{a}^\dagger_{\boldsymbol{p}_2-\boldsymbol{q}} \hat{a}_{\boldsymbol{p}_2} \hat{a}_{\boldsymbol{p}_1}, \tag{1.11}$$

where $\tilde{U}(\boldsymbol{q}) = g + \tilde{U}_{dd}(\boldsymbol{q})$. Assuming a condensate in $p = 0$ (i.e. an homogeneous BEC), we may approximate $\hat{a}_0 = \hat{a}_0^\dagger = \sqrt{N}$, where $N = n_0 V$ is the number of particles. Expanding up to second order $\hat{a}_{\boldsymbol{p}\neq 0}$ we get up to a constant:

$$\hat{H} = \sum_{\boldsymbol{p}\neq 0} \frac{p^2}{2m} \hat{a}^\dagger_{\boldsymbol{p}} \hat{a}_{\boldsymbol{p}} + \frac{n_0}{2} \sum_{\boldsymbol{p}} \tilde{U}(\boldsymbol{p}) \left(2\hat{a}^\dagger_{\boldsymbol{p}} \hat{a}_{\boldsymbol{p}} + \hat{a}^\dagger_{\boldsymbol{p}} \hat{a}^\dagger_{-\boldsymbol{p}} + \hat{a}_{\boldsymbol{p}} \hat{a}_{-\boldsymbol{p}} \right). \tag{1.12}$$

As one can easily see this Hamiltonian just couples $\boldsymbol{p}$ with $-\boldsymbol{p}$. This means that we can diagonalise using a Bogoliubov transformation for each $\boldsymbol{p}$. We do not do it here in detail because this is the standard Bogoliubov-transformation procedure. It is more important to have a look to the dispersion resulting from this diagonalisation:

$$\epsilon(\boldsymbol{p}) = \sqrt{\frac{p^2}{2m} \left[\frac{p^2}{2m} + 2n_0 \left(g + \tilde{U}_{dd}(\boldsymbol{p}) \right) \right]} \tag{1.13}$$

Note that due to the momentum dependence of the DDI, the dispersion now has an anomalous momentum dependence. Let us see what happens for $p \to 0$. In that case we may approximate

$$\epsilon(\boldsymbol{p}) = pc_{s0}\sqrt{1+\epsilon_{dd}(3\cos^2\theta_p - 1)} \tag{1.14}$$

where $c_{s0} = \sqrt{\frac{gn_0}{m}}$ is the sound velocity in absence of DDI. Note that for $\theta_p = \pi/2$, i.e. for momenta perpendicular to the dipolar orientation, $\epsilon(\boldsymbol{p}) = pc_{s0}\sqrt{1-\epsilon_{dd}}$. As a result, for $\epsilon_{dd} > 1$ some excitation modes are purely imaginary. Hence, the homogeneous 3D dipolar BEC is dynamically unstable against very long-wave length excitations. We will denote this instability "phonon instability".

1.2.3 Trapped gases: geometry-dependent stability

The phonon instability scenario resembles the case of $a < 0$ where due to similar reasons, an homogenous BEC is also unstable (that is easy to see from (1.13) taking $g < 0$ and $\tilde{U}_{dd} = 0$). However, in a trap, quantum pressure may stabilise the BEC for small atom numbers ($N < N_c$). For an isotropic harmonic trap of frequency ω, $N_c|a|/a_{\rm ho} = 0.58$, where $a_{\rm ho} = \sqrt{\hbar/(m\omega)}$ is the oscillator length (Ruprecht *et al.*, 1995). For anisotropic traps, the dependence on the trap geometry is weak (Gammal *et al.*, 2001).

The situation is very different in dipolar BECs due to the anisotropy of the DDI. We shall see in the following that the trap geometry determines crucially the stability of a dipole BEC. In order to see that, let us consider for simplicity a cylindrically symmetric trap, with a symmetry axis z coinciding with the dipole orientation. The axial (resp. radial) trapping frequency is denoted ω_z (resp. ω_ρ), such that $\lambda = \omega_z/\omega_\rho$. Let us consider a Gaussian variational ansatz of the form:

$$\psi(\rho, z) = \frac{\sqrt{N}}{\pi^{3/4} l_\rho l_z^{1/2}} e^{-z^2/2l_z^2} e^{-\rho^2/2l_\rho^2}. \tag{1.15}$$

Note that the cloud aspect ratio $\kappa = l_\rho/l_z$ is in general different than the trap aspect ratio $\lambda^{1/2}$.

We may evaluate the expression for the total energy as a function of l_ρ and l_z: $E = E_{kin} + E_{trap} + E_{sr} + E_{dd}$, where

$$E_{kin} = \frac{\hbar^2}{2m}\int d^3\boldsymbol{r}|\nabla\psi|^2 = \frac{N\hbar^2}{2m}\left\{\frac{1}{l_z^2} + \frac{2}{l_\rho^2}\right\} \tag{1.16}$$

is the kinetic energy,

$$E_{trap} = \int d^3\boldsymbol{r} V_{trap}(\boldsymbol{r}) n(\boldsymbol{r}) = \frac{Nm}{4}\left\{2\omega_\rho^2 l_\rho^2 + \omega_z^2 l_z^2\right\} \tag{1.17}$$

is the trap energy ($n(\boldsymbol{r}) = |\psi(\boldsymbol{r})|^2$), and

$$E_{sr} = \frac{g}{2}\int d^3\boldsymbol{r} n(\boldsymbol{r})^2 = \frac{gN^2}{2(2\pi)^{3/2} l_z l_\rho^2} \tag{1.18}$$

is the contact interaction energy.

Finally E_{dd} is the mean DDI, which is especially interesting for us:

$$E_{dd} = \frac{1}{2}\int d^3\boldsymbol{r}\int d^3\boldsymbol{r}' U_{dd}(\boldsymbol{r}-\boldsymbol{r}')n(\boldsymbol{r}')n(\boldsymbol{r}). \tag{1.19}$$

This expression is best evaluated in momentum space:

$$E_{dd} = \frac{1}{2}\int \frac{d^3\boldsymbol{k}}{(2\pi)^3}\tilde{U}_{dd}(\boldsymbol{k})|\tilde{n}(\boldsymbol{k})|^2, \tag{1.20}$$

where $\tilde{n}(\boldsymbol{k}) = N\exp[-k_z^2 l_z^2/4 - k_\rho^2 l_\rho^2/4]$ is the Fourier transform of the density. Let $q_j = k_j l_j$ $(j = \rho, z)$, then

$$\begin{aligned} E_{dd} &= \frac{C_{dd}N^2}{6(2\pi)^3 l_\rho^2 l_z}\int d^3\boldsymbol{q}e^{-q^2/2}\frac{2\kappa^2\cos^2\theta_q - \sin^2\theta_q}{\kappa^2\cos^2\theta_q + \sin^2\theta_q} \\ &= \frac{C_{dd}N^2}{3(2\pi)^{3/2} l_\rho^2 l_z}\left\{\frac{2\kappa^2+1}{\kappa^2-1} - \frac{3\kappa^2}{(\kappa^2-1)^{3/2}}\arctan[\sqrt{\kappa^2-1}]\right\} \\ &= \frac{C_{dd}N^2}{3(2\pi)^{3/2} l_\rho^2 l_z} f(\kappa). \end{aligned} \tag{1.21}$$

The function $f(\kappa)$ is monotonically growing, has asymptotic values $f(0) = -1$ and $f(\infty) = 2$, and vanishes for $\kappa = 1$ (implying that for an isotropic density distribution the mean DDI averages to zero). For a cigar-shape BEC elongated along the dipole orientation ($\kappa < 1$), $E_{dd} < 0$, i.e. the DDI is essentially attractive. This is intuitively easy to understand, since in that case the dipoles see each other head with tail in average. On the contrary, for an oblate trap ($\kappa > 1$) $E_{dd} > 0$, i.e. the DDI is essentially repulsive. This is again intuitive, because the dipoles see each other side by side in average.

The physics of the dipolar BEC, and in particular its stability and the relation between trap and cloud aspect ratio, may be obtained by minimising the energy E with respect to l_ρ and l_z for fix N, ω_ρ and ω_z. A stable BEC is characterised by the presence of a (at least local) minimum of E for finite values of l_ρ and l_z (a local minimum means actually a metastable solution, but we shall consider the lifetime as infinite). The disappearance of such a minimum marks the point of destabilisation of the condensate.

For purely dipolar interactions (i.e. $a = 0$) there is a critical $\lambda_{cr} \simeq 5.2$ (Santos *et al.*, 2000; Góral and Santos, 2002; Yi and You, 2001; Eberlein *et al.*, 2005; Koch *et al.*, 2005), such that for $\lambda < \lambda_{cr}$ the condensate is unstable for a sufficiently large number of particles (i.e. quite similar as for the $a < 0$ case without DDI). On the contrary if $\lambda > \lambda_{cr}$ (sufficiently pancake trap), there is in principle no critical number of particles. In other words, the phonon-like instability is geometrically stabilised (however another type of instability may occur in that case, as we shall see later). Note that, interestingly, the critical trap aspect ratio is $\lambda_{cr}^{1/2} = 2.28$, i.e. a slightly pancake trap, and not, as one could naively think, a spherical trap. This is because for large N, $\kappa \to 1$ when $\lambda \to \lambda_{cr}$, i.e. the trap is pancaked but the BEC cloud for λ_{cr} is spherical (note that this can never happen in non-dipolar BECs).

Let us analyse what happens when $a \neq 0$. Repulsive short-range interactions ($a > 0$) may stabilise (up to some point) an unstable dipolar BEC. Note also that even if the mean DDI is repulsive, a sufficiently strong attractive contact interaction ($a < 0$) may destabilise the BEC. Hence, for non-zero contact interactions, we may expect that for a given λ, there exists a critical value $a_{\rm crit}(\lambda)$ such that for $a < a_{\rm crit}(\lambda)$ the dipolar BEC is unstable.

For a given N, the actual curve $a_{\rm crit}(\lambda)$ must be determined numerically (Bohn *et al.*, 2009). This curve decreases monotonously with λ. For very prolate traps ($\omega_z \ll \omega_\rho$), $E_{dd} < 0$, and one expects that a positive a is necessary to stabilise the BEC (hence $a_{\rm crit} > 0$). On the contrary, for very oblate traps ($\omega_z \gg \omega_\rho$), $E_{dd} > 0$ and hence one needs a sufficiently large $a < 0$ to destabilise the BEC (i.e. $a_{\rm crit} < 0$).

In particular, in the limit $N \to \infty$, the asymptotic behaviour of the $a_{\rm crit}$ curve ($a^{\infty}_{\rm crit}(0) = a_{\rm dd} \equiv mC_{dd}/12\pi\hbar^2$ and $a^{\infty}_{\rm crit}(\infty) = -2a_{\rm dd}$) can be easily understood, as only the sign of the interaction term $E_{sr} + E_{dd}$ (which scales as N^2 and not as N like E_{kin} and E_{trap}) determines the stability. For an extremely pancake-shaped trap $\lambda \to \infty$, the cloud has an aspect ratio $\kappa \to \infty$, and, as $f(\kappa \to \infty) = -2$, the BEC is (meta-)stable only if $a > -2a_{\rm dd}$. In the same way, one readily understand that for $\lambda \to 0$, the critical scattering length is $a_{\rm dd}$.

In (Koch *et al.*, 2005), the influence of the trapping geometry on the stability of a ^{52}Cr BEC was investigated experimentally. In particular, that experiment determined the curve $a_{\rm crit}(\lambda)$. A typical measurement is shown in Fig. 1.3. Note that, although the main qualitative features are recovered by a simple Gaussian ansatz, to calculate the exact stability threshold, one needs to resort to a numerical solution of the non-local GPE (1.10) (Bohn *et al.*, 2009).

When the system becomes unstable (due to this phonon-like instability) it collapses. This collapse (which is induced by a change in a by means of Feshbach resonances) has been recently observed experimentally (Lahaye *et al.*, 2008). Interestingly the post-collapse images present a cloverleaf pattern caused by the anisotropic collapse of the system (see Fig. 1.4). When the atomic density grows due to the attractive interaction, three-body losses predominantly occur in the high-density region. The centripetal force is then decreased, and the atoms that gathered in this narrow central region are ejected due to the quantum pressure arising from the uncertainty principle. The kinetic energy is supplied by the loss of the negative interaction energy. As the collapse occurs mainly in the $x - y$ direction due to anisotropy of the DDI (in the absence of inelastic losses, the condensate would indeed become an infinitely thin cigar-shaped cloud along z), and therefore the condensate explodes essentially radially, producing the anisotropic shape of the cloud.

Note finally, that phonon-instability does not necessarily lead to collapse in 2D geometries, and may be accompanied by the formation of stable 2D solitons (Nath *et al.*, 2009), which are discussed in Sec. 1.2.6.

1.2.4 Trapped gases: Thomas-Fermi regime

As for the case of non-dipolar BECs, for sufficiently strong interactions, we may neglect quantum pressure, and consider the Thomas-Fermi (TF) regime.

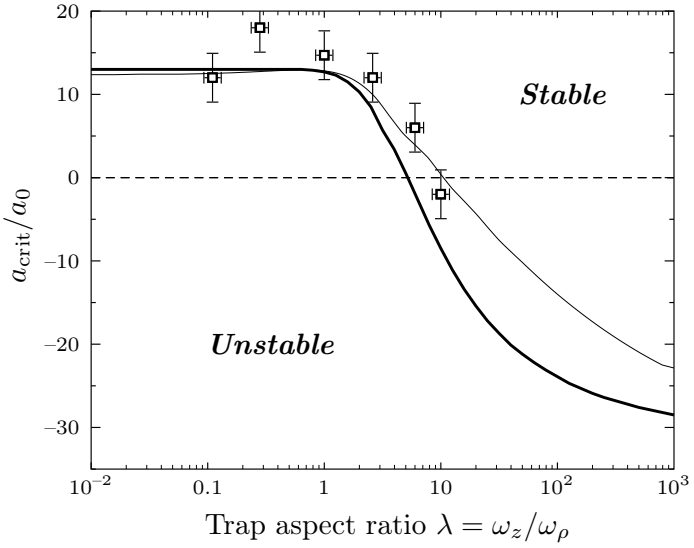

Fig. 1.3 Stability diagram of a dipolar condensate in the plane (λ, a). The dots with error bars correspond to the experimental data (Koch *et al.*, 2005); the thick solid line to the threshold $a_{\rm crit}(\lambda)$ obtained using the Gaussian ansatz (1.15) with $N = 20,000$; the thin solid line to the numerical solution of the GPE (1.10) (Bohn *et al.*, 2009). Figure from Ref. (Lahaye *et al.*, 2009).

$$\mu = V_{trap}(\boldsymbol{r}) + g|\psi(\boldsymbol{r},t)|^2 + \int d^3\boldsymbol{r}' U_{dd}(\boldsymbol{r}-\boldsymbol{r}')|\psi(\boldsymbol{r}',t)|^2. \tag{1.22}$$

Amazingly, the TF solution for the trapped BEC has the same inverted parabola shape as for the non-dipolar case (Eberlein *et al.*, 2005; O'Dell *et al.*, 2004). This is a quite non-trivial result, taking into account the rather complicated form of Eq. (1.22)!

In particular, the ground state density in a cylindrically-symmetric trap (with frequencies ω_ρ and $\omega_z = \lambda\omega_\rho$ as above) has the form:

$$n(\boldsymbol{r}) = n_0 \left(1 - \frac{\rho^2}{R_\rho^2} - \frac{z^2}{R_z^2}\right), \tag{1.23}$$

for $n(\boldsymbol{r}) \geqslant 0$, where $n_0 = 15N/(8\pi R_\rho^2 R_z)$. These expressions are the same as for the non-dipolar case, but the explicit expressions for the TF radii are of course different. They may be obtained by substituting (1.23) into (1.22) (Eberlein *et al.*, 2005; O'Dell *et al.*, 2004):

$$R_\rho = \left[\frac{15gN\kappa}{4\pi m\omega_\rho^2}\left\{1 + \varepsilon_{\rm dd}\left(\frac{3}{2}\frac{\kappa^2 f(\kappa)}{\kappa^2-1} - 1\right)\right\}\right]^{1/5}, \tag{1.24}$$

with $\kappa = R_\rho/R_z$, and $f(\kappa)$ as above.

Interestingly, one may obtain a closed transcendental equation which links the BEC aspect ratio (κ) and the trap aspect ratio $(\lambda^{1/2})$:

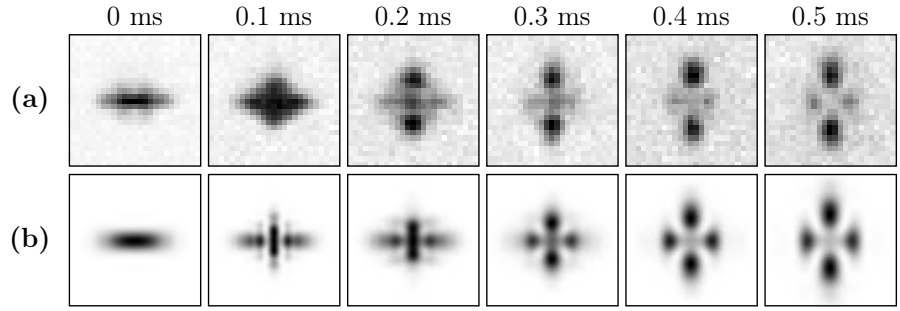

Fig. 1.4 (a) Experimental images of a dipolar condensate after collapse and explosion, as a function of the time $t_{\rm hold}$ between the crossing of the critical scattering length for instability and the release from the trap. The time of flight is 8 ms. (b) Results of a numerical simulation of the collapse dynamics, without any adjustable parameter. The field of view is 130μm $\times$ 130μm. Figure from Ref. (Lahaye *et al.*, 2008).

$$3\kappa\varepsilon_{\rm dd}\left[\left(\frac{\lambda^2}{2}+1\right)\frac{f(\kappa)}{\kappa^2-1}-1\right]+(\varepsilon_{\rm dd}-1)(\kappa^2-\lambda^2)=0. \tag{1.25}$$

A plot of the condensate aspect ratio as a function of $\varepsilon_{\rm dd}$ is shown in figure 1.5.

The latter equation is quite interesting, since it may actually lead to more than one solution κ for a given lambda (see Fig. 1.5). One of the solutions (let us call it the normal solution) is stable (or metastable). Interestingly for $a = 0$ this solution just exists for $\lambda^{1/2} > \lambda_{cr}^{1/2} = 2.28$, i.e. exactly the stability criterion obtained in the previous section for the Gaussian Ansatz. On the contrary, the second solution, which appears for a sufficiently large DDI ($\epsilon_{dd} > 1$) is characterised by two main features. On one hand it corresponds to a less pancake solution. On the other hand this anomalous solution is unstable. Hence, contrary to what it may have been expected from our discussion of the geometric stabilisation in the previous section a TF solution is not stable for arbitrary large number of particles, being unstable against the nucleation of anomalous "bubbles", which will eventually collapse. This means that, contrary to the instability discussed in previous sections, we are not dealing here with the instability of phonon-like excitations, i.e. excitations with a wavelength comparable to that of the condensate. On the contrary, intermediate finite wavelengths become here unstable, leading to local (and not global) collapses. This instability is directly related with the roton instability which we will discuss in the next section.

1.2.5 Roton-like dispersion law

In the previous section we have seen that a dipolar BEC may become eventually unstable even for pancake traps, i.e. the BEC may be geometrically stabilised only to some extent. We shall now try to understand the nature of this instability. For simplicity of our discussion we shall concentrate in a dipolar BEC harmonically confined in the dipole direction (z-axis) and uniform on the xy plane. The corresponding nonlocal GPE reads then

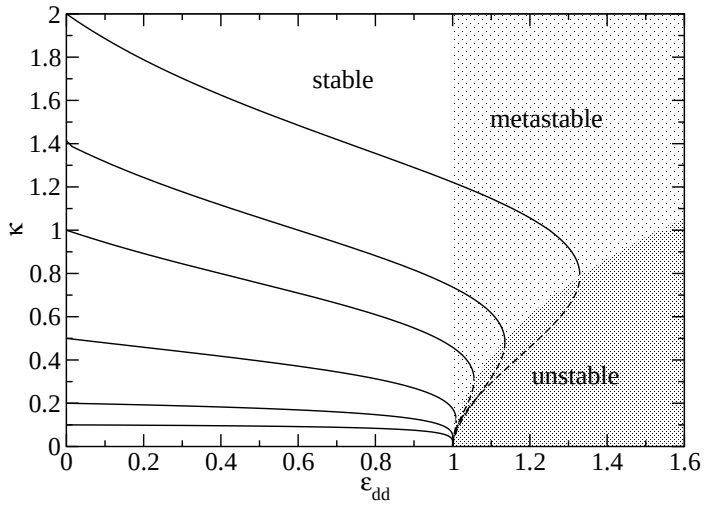

Fig. 1.5 Aspect ratio κ of the condensate as a function of the dipole-dipole to s-wave coupling ratio $\varepsilon_{\rm dd}$. Each line is for a different trap aspect ratio $\lambda = \omega_z/\omega_x$, which can be read off by noting that $\kappa(\varepsilon_{\rm dd} = 0) = \gamma$. When $0 < \kappa < 1$ the condensate is prolate; for $\kappa > 1$ it is oblate. Likewise, for $0 < \gamma < 1$ the trap is prolate, and when $\gamma > 1$ the trap is oblate. Figure courtesy of C. Eberlein.

$$i\hbar\frac{\partial}{\partial t}\psi(\boldsymbol{r},t) = \left[-\frac{\hbar^2}{2m}\nabla^2 - \mu + \frac{m\omega^2 z^2}{2} + g|\psi(\boldsymbol{r},t)|^2 + \int d\boldsymbol{r}' U_{dd}(\boldsymbol{r}-\boldsymbol{r}')|\psi(\boldsymbol{r}',t)|^2\right]\psi(\boldsymbol{r},t). \tag{1.26}$$

where ω is the trap frequency. The ground-state wave-function is independent of the in-plane coordinates and can be written as $\psi_0(z)$. Then, integrating over the in-plane coordinates in the DDI, we obtain a 1D equation similar to the a GP equation for a 1D system with short-range interactions:

$$\left[\frac{-\hbar^2}{2m}\frac{d^2}{dz^2} + \frac{m\omega^2 z^2}{2} + (g+g_d)|\psi_0|^2 - \mu\right]\psi_0(z) = 0 \tag{1.27}$$

where $g_d = 8\pi C_{dd}/3$. In the following we consider the case $(g + g_d) > 0$, where $\mu > 0$. For $\mu \gg \omega$ the BEC is in the TF regime with a density profile $n_0(z) = n_0(1 - z^2/L^2)$ with a central density $n_0 = \mu/(g + g_d)$ and a TF radius $L = (2\mu/m\omega^2)^{1/2}$.

We are interested in the elementary excitations on top of ψ_0, which we shall study by means of a Bogoliubov-de Gennes analysis. We look for solutions of the form:

$$\psi(\boldsymbol{r},t) = \psi_0(z) + u(z)e^{i\boldsymbol{q}\cdot\boldsymbol{\rho}}e^{-i\omega t} + v^*(z)e^{-i\boldsymbol{q}\cdot\boldsymbol{\rho}}e^{-i\omega t} \tag{1.28}$$

where $u(z)$ and $v(z)$ are complex amplitudes of small oscillations of the condensate around the ground state. The excitations are characterised by a momentum q of the in-plane free motion. Introducing the convenient functions $f_\pm = u \pm v$ the Bogoliubov-de Gennes equations become of the form:

$$\hbar\omega f_-(z) = \hat{H}_{kin} f_+(z), \tag{1.29}$$
$$\hbar\omega f_+(z) = \hat{H}_{kin} f_-(z) + \hat{H}_{int}[f_-(z)], \tag{1.30}$$

where

$$\hat{H}_{kin} = \frac{\hbar^2}{2m}\left[-\frac{d^2}{dz^2} + q^2 + \frac{\nabla^2\psi_0}{\psi_0}\right], \tag{1.31}$$
$$\hat{H}_{int}[f_-] = 2(g+g_d)\psi_0^2(z) f_-(z) - \frac{3}{2} q g_d \psi_0(z) \int_{-\infty}^{\infty} dz' \psi_0(z') \exp[-q|z-z'|] f_-(z'), \tag{1.32}$$

are respectively the kinetic and the interaction operator. For each q we have different eigen-energies $\hbar\omega$. The most interesting is the lowest branch $\omega_0(q)$, which provides us the dispersion law.

The integral term of $H_{int}[f_-]$ originates from the nonlocal character of the DDI and gives rise to the momentum dependence of an effective coupling strength. In the limit of low in-plane momenta $qL \ll 1$, this term can be omitted. In this case, excitations of the lowest branch are essentially 2D and the effective coupling strength corresponds to repulsion. We then recover the Bogoliubov-de Gennes equations for the excitations of a trapped non-dipolar BEC with a coupling constant $(g + g_d) > 0$. In particular, at $q \to 0$, we recover phonons propagating in the xy-plane, with a sound-velocity $c_s = (2\mu/3m)^{1/2}$.

The situation is very different for $qL \gg 1$. In that case, the excitations become 3D and the effective coupling strength is reduced to $(2g - g_d)$, as one can put $z_0 = z$ in the arguments of f and ψ_0 in the integrand of Eq. (1.32). We hence recover once more the Bogoliubov-de Gennes equations for excitations of a non-dipolar condensate but now with a coupling constant $(2g - g_d)$. If the parameter $\beta = g_d/g < 2$, this coupling constant is positive and one has excitation energies which are real and positive for any momentum q and condensate density n_0. For $\beta > 2$, the coupling constant is negative and at a sufficiently large density the condensate becomes dynamically unstable with regard to creation of high momentum excitations.

We hence see that something quite remarkable may happen due to the momentum-dependence of the DDI. For low momenta we may have stable phonons (i.e. no phonon instability as that discussed in Sec. 1.2.2), but the BEC may be anyway unstable at finite momenta. Fig. 1.6 shows a typical dispersion law as directly obtained from the Bogolibov-de Gennes equations. Note the significant departure when compared to the usual Bogoliubov spectrum. The usual Bogoliubov spectrum is characterized by a phonon dispersion ($\sim q$) at low q and a single-particle dispersion ($\sim q^2$) at large momenta. On the contrary the dispersion law in a dipolar BEC may become non-monotonical. For in-plane momenta $qL \ll 1$ we have 2D phonon-like excitations, for $qL > 1$, excitations are 3D and the interparticle repulsion is reduced. This decreases the excitation energy under an increase of q. The dispersion reaches a minimum and then starts to grow as the excitations enter the single-particle regime. This minimum resembles that found in Helium physics (although the physics behind is actually rather different), and hence we shall call it in the following roton-like minimum. If this roton touches zero, the BEC will then become dynamically unstable.

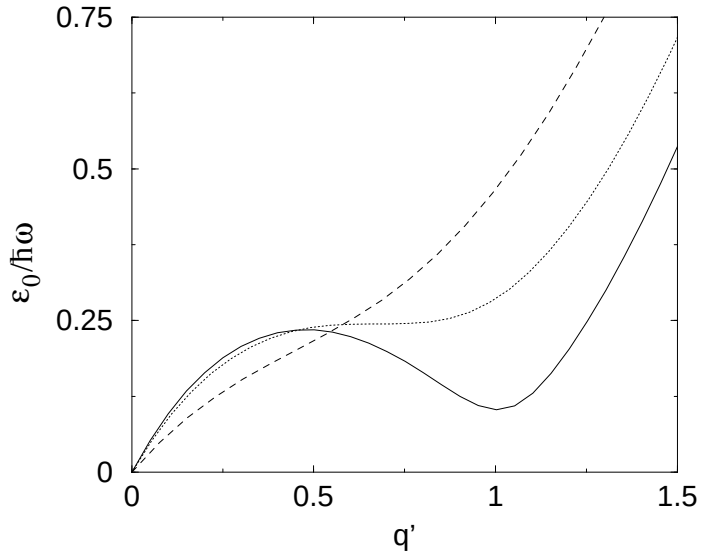

Fig. 1.6 Typical dispersion law $\epsilon_0(q)$ ($q' \equiv ql_0$, with $l_0 = \sqrt{\hbar/m\omega}$) for a non-dipolar gas ($\beta = 0$) (dashed), and for a dipolar gas right before developing the roton (dotted) and with a developed roton-like minimum (solid). See Ref. (Santos *et al.*, 2003) for more details.

The existence of a roton-like minimum is a remarkable characteristic feature of dipolar condensates. Dipolar BEC constitutes indeed the first example of a weakly-interacting gas which may show a roton-like minimum in the dispersion, which up to now has been observed only in the relatively more complicated physics of liquid Helium. Moreover, in contrast to the Helium case, by varying the density, the frequency of the confinement, and the short-range coupling, one can easily manipulate and control the spectrum, making the roton minimum deeper or shallower. One can also eliminate it completely and get the Bogoliubov-type spectrum or, on the opposite, reach the point of instability.

The roton-like minimum has not been yet observed experimentally, although ongoing experiments in this direction are performed in Stuttgart. If created the presence of a roton-like minimum may be revealed in various ways: reduction of the superfluid critical velocity (Santos *et al.*, 2003), "halo" effect at finite temperature in time-of-flight images (Wang and Demler, 2010), or the dramatically altered response of the system against a periodic driving in the presence of a roton-like minimum (Nath and Santos, 2010).

Let us finally comment on the fate of the condensate after the roton instability sets in. The presence of dynamical instability at finite momentum, seems to suggest that the system may develop a modulation with a finite wavelength provided by the inverse roton momentum. if this were so, this could open a route towards supersolidity (one of the holy grails of condensed matter physics), which is a superfluid with both diagonal and non-diagonal long-range order. Unfortunately, it seems that the ultimate answer

to this problem is negative. The formation of a modulation is just a transitien which quickly leads to the formation of local collapses (Dutta and Meystre, 2007; Komineas and Cooper, 2007; Shlyapnikov and Pedri, 2006). However, it has been shown recently that introducing a cut-off of the dipole-dipole interaction at short distances may stabilize the supersolid pattern. This may occur by properly tailoring inter-molecular interactions (Wang, 2010). Another possibility is provided by the dipole-blockade in Rydberg gases, as recently studied in Refs. (Henkel *et al.*, 2010; Cinti *et al.*, 2010).

1.2.6 Solitons

The 1D Gross-Pitaevskii equation (with $a < 0$) supports the existence of solitons, i.e. localized waves that travel with neither attenuation nor change of shape due to the compensation between dispersion and nonlinearity (Zakharov and Shabat, 1972). Solitons have been indeed observed in quasi-1D condensates with $a < 0$ (Strecker *et al.*, 2002; Khaykovich *et al.*, 2002). The quasi-1D condition requires a tight transversal harmonic trap of frequency $\omega_\perp$ such that $\hbar\omega_\perp$ exceeds the mean-field interaction energy. This in turn demands the transversal BEC size to be smaller than the soliton width. When this condition is violated the soliton becomes unstable against transversal modulations, and hence multi-dimensional solitons are not stable in non-dipolar BECs. Remarkably the latter is not necessarily true in dipolar BECs, where as a consequence of the non-local non-linearity 2D bright solitary waves may become stable under appropriate conditions (Pedri and Santos, 2005). In the following we shall discuss the scenario studied by Tikhonenkov *et al.* (Tikhonenkov *et al.*, 2008), since it is closer to possible actual experiments (with Chromium) than the original proposal of Ref. (Pedri and Santos, 2005).

The possibility of obtaining stable solitary waves may be easily understood from a simplified discussion where we consider no trapping in the xz-plane and a strong harmonic confinement with frequency ω_y in the y-direction. The dipole are oriented along the z direction, i.e. within on the plane of the trap. A good insight on the stability of the solitons may be obtained from a simple Gaussian ansatz:

$$\psi(\boldsymbol{r}) = \frac{1}{l_y^{3/2}} \frac{1}{\pi^{3/4}\Lambda_x\Lambda_z} e^{\frac{1}{2l_y^2}\left(\frac{x^2}{\Lambda_x^2}+\frac{z^2}{\Lambda_z^2}+y^2\right)} \tag{1.33}$$

where $l_y = \sqrt{\hbar/m\omega_y}$ is the oscillator length along the transverse direction, and $\Lambda_{x,z}$ are variational parameters that determine the width of the width of the Gaussian (in l_y units). We may insert this ansatz into the Hamiltonian of the nonlocal GPE, obtaining (apart from unimportant constants):

$$\epsilon \equiv \frac{E}{N\hbar\omega_y} = \frac{1}{4(\Lambda_x^2+\Lambda_z^2)} + \frac{\tilde{g}}{4\pi\Lambda_x\Lambda_z}\left[1+\epsilon_{dd}h\left(\frac{\Lambda_x}{\Lambda_z},\frac{1}{\Lambda_z}\right)\right], \tag{1.34}$$

where $\tilde{g} = \frac{m}{\hbar^2}\frac{Ng}{\sqrt{2\pi}l_y}$, and

$$h(\alpha,\beta) = -1 + 3\int_0^1 ds \frac{3\alpha\beta s^2}{\left[1+\alpha^2-1)s^2\right]^{1/2}\left[1+\beta^2-1)s^2\right]^{1/2}}. \tag{1.35}$$

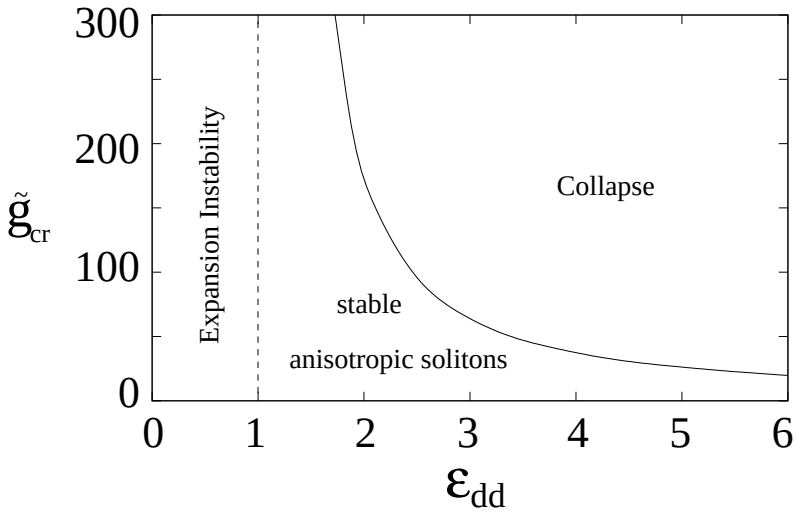

Fig. 1.7 Stability diagram of an anisotropic soliton as a function of $\varepsilon_{\rm dd}$ and $\tilde{g}_{\rm cr} = g_{\rm cr}/\sqrt{2\pi}l_z$, where for $g > g_{\rm cr}$ the soliton is unstable against collapse even for $\varepsilon_{\rm dd} > 1$. Figure from Ref. (Nath *et al.*, 2009).

Let us consider first what happens for non-dipolar gases. In that case $\epsilon_{dd} = 0$ and

$$\epsilon(\Lambda = \Lambda_x = \Lambda_z) = \frac{(1 + \tilde{g}/2\pi)}{2\Lambda^2}, \tag{1.36}$$

hence depending on the sign of $1 + \tilde{g}/2\pi$ the system minimises the energy either by expanding without limits, or by contracting without limits. The localised solution is hence unstable. This is once more the well-known instability of solitons in 2D.

The extra term provided by the DDI is quite interesting, since it introduces an additional dependence on $\Lambda_{x,z}$. This allows (under appropriate conditions) for a minimum in the energy, and hence for a stable self-localised solution! This minimum is characterised by its equilibrium widths Λ_{x0} and $\Lambda_{z,0}$. Note that they are in general not equal. This asymmetry comes of course from the fact that the dipole is along the z direction. In Fig. 1.7 (Nath *et al.*, 2009) we show the stability diagram as a function of $\tilde{g}$ and ϵ_{dd}. There we observe two instability regions for 2D solitons (against collapse and against unlimited expansion). For $\epsilon_{dd} > 1$, there is a critical universal value $\tilde{g}_{cr}(\beta) \equiv gN_{cr}/\sqrt{2\pi}l_z$ such that for $N > N_{cr}$ the minimum of $E(\Lambda_x, \Lambda_z)$ disappears. As a consequence, stable 2D anisotropic self-localised solutions are stable only for a number of particles per soliton below a critical number N_{cr}, which decreases for larger ϵ_{dd}. Beyond this number the 2D soliton collapses. This result is also verified by a direct simulation of the 3D nonlocal Gross-Pitaevskii equation.

In this simplified discussion we have assumed that the problem remains 2D. If the interactions increase the problem becomes 3D, and one may show that the condensate becomes eventually unstable (Pedri and Santos, 2005; Tikhonenkov *et al.*, 2008).

A major difference between bright solitons in non-dipolar and dipolar BECs concerns the soliton-soliton scattering properties. Whereas 1D solitons in non-dipolar

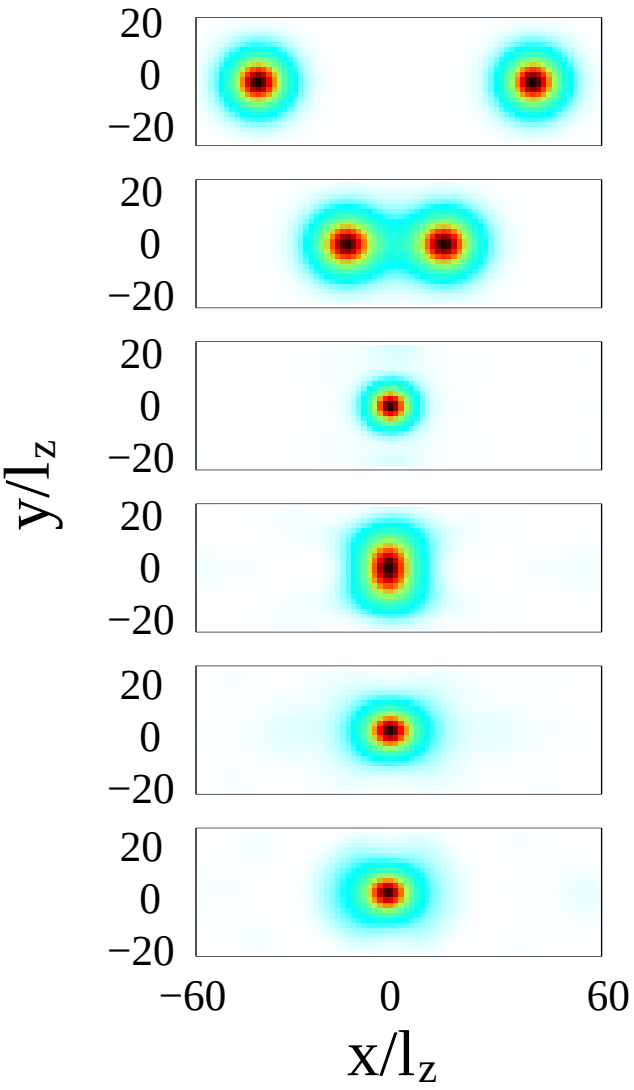

Fig. 1.8 Density plot of the fusion of two dipolar 2D solitons. See Ref. (Pedri and Santos, 2005) for details.

BECs scatter elastically, the scattering of dipolar solitons is inelastic due to the lack of integrability (Krolikowski *et al.*, 2001). The solitons may transfer centre-of-mass energy into internal vibrational modes, resulting in intriguing scattering properties, including soliton fusion (Pedri and Santos, 2005) (see Fig. 1.8), the appearance of strong inelastic resonances (Nath *et al.*, 2007), and the possibility of observing 2D-soliton spiraling as that already observed in photo-refractive materials (Shih *et al.*, 1997).

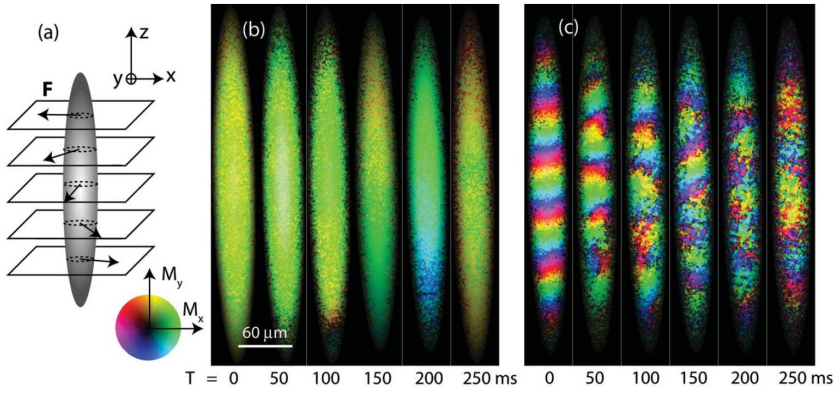

Fig. 1.9 Spontaneous dissolution of helical textures in a quantum degenerate ^{87}Rb spinor Bose gas. A transient magnetic field gradient is used to prepare transversely magnetised (b) uniform or (a),(c) helical magnetisation textures. The transverse magnetisation column density after a variable time T of free evolution is shown in the imaged $x-z$ plane, with orientation indicated by hue and amplitude by brightness (colour wheel shown). (b) A uniform texture remains homogeneous for long evolution times, while (c) a helical texture with pitch $\lambda = 60\,\mu$m dissolves over ~ 200 ms, evolving into a sharply spatially modulated texture. Figure from Ref. (Vengalattore *et al.*, 2008).

1.2.7 Dipolar effects in spinor condensates

Let us finish the discussion on dipolar BEC with some brief comments about dipolar effects in spinor BECs, i.e. in BECs formed by atoms with non-zero spin. Dipolar effects may lead to very interesting phenomena in spinor BECs (for a review see e.g. (Lahaye *et al.*, 2009)) but here we shall focus only in a particular effect which resembles the famous Einstein-de Haas effect.

In a spinor BEC we have various Zeeman sub-levels with quantum number m. The short-range interactions may hence occur in different s-wave scattering channels with different total angular momentum which for the case of bosons must be an even number (i.e. for spin-1 bosons we have just two scattering channels, namely $F=0$ and $F=2$) (Ho, 1998). For each scattering channel we have an associated s-wave scattering length a_F. The short-range interactions necessarily preserve the spin projection S_z along the quantisation axis.

The DDI for a spinor BEC is of the form

$$\hat{V}_{\rm dd} = \frac{C_{\rm dd}}{2}\int {\rm d}\boldsymbol{r}\int {\rm d}\boldsymbol{r}'\frac{1}{|\boldsymbol{r}-\boldsymbol{r}'|^3}\hat{\psi}^\dagger_m(\boldsymbol{r})\hat{\psi}^\dagger_{m'}(\boldsymbol{r}') \\ \left[\boldsymbol{S}_{mn}\cdot\boldsymbol{S}_{m'n'} - 3(\boldsymbol{S}_{mn}\cdot\boldsymbol{e})(\boldsymbol{S}_{m'n'}\cdot\boldsymbol{e})\right]\hat{\psi}_n(\boldsymbol{r})\hat{\psi}_{n'}(\boldsymbol{r}'), \tag{1.37}$$

where $\boldsymbol{S} = (S_x, S_y, S_z)$ are the spin-F matrices, $C_{\rm dd} = \mu_0\mu_B^2 g_F^2/4\pi$, and $\boldsymbol{e} = (\boldsymbol{r}-\boldsymbol{r}')/|\boldsymbol{r}-\boldsymbol{r}'|$.

Interestingly, contrary to the short-range interaction the dipole-dipole interaction does not necessarily conserve the spin projection along the quantisation axis due to

the anisotropic character of the interaction. In particular, if the atoms are initially prepared into a maximally stretched state, say $m_F = -F$, short-range interactions cannot induce any spinor dynamics due to the above mentioned conservation of total magnetisation S_z. Dipole-dipole interactions, on the contrary may induce a transfer into m_F+1. If the system preserves cylindrical symmetry around the quantisation axis, this violation of the spin projection is accompanied by a transfer of angular momentum to the centre of mass, resembling the well known Einstein-de Haas effect (Santos and Pfau, 2006; Kawaguchi *et al.*, 2006). Due to this transfer an initially spin-polarised dipolar condensate can generate dynamically vorticity.

Unfortunately, the Einstein-de Haas effect is destroyed in the presence of even rather weak magnetic fields. Typically, magnetic fields well below 1 mG are necessary to observe the effect. Due to the dominant role of Larmor precession, and invoking rotating-wave-approximation arguments, the physics must be constrained to manifolds of preserved magnetisation (this may be overcome in tight 2D optical lattices, as suggested by recent results at Paris Nord (Pasquiou *et al.*, 2011).

However the dipole-dipole interaction may have observable effects also under conserved magnetisation S_z, even for alkali spinor condensates. The mechanism for spinor dynamics in spinor BECs is the so-called spin-changing collisions, i.e. collisions that conserve S_z but do not conserve the relative population of the different Zeeman components. Spin-changing collisions are characterised by an energy scale proportional to the difference between scattering lengths at different channels. This difference is typically very small, and hence the energy of spin-changing collisions is very low. This is particularly so for the case of ^{87}Rb $F = 1$. As a consequence the spinor physics may be significantly modified by the presence of other small energy scales and in particular the DDI. Recent experiments at Berkeley (Vengalattore *et al.*, 2008) have demonstrated the dipolar character of spin-1 ^{87}Rb spinor BECs. In particular, these experiments show the spontaneous decay of helical spin textures (externally created by magnetic field gradients) toward a spatially modulated structure of spin domains (see Fig. 1.9). The formation of this modulated phase has been ascribed to magnetic dipolar interactions that energetically favour short-wavelength domains over the long-wavelength spin helix. Interestingly, the reduction of dipolar interactions (by means of radio-frequency pulses) results in a suppression of the modulation.

1.3 Dipolar gases in optical lattices

At this point we shall discuss some of the fascinating effects introduced by the DDI in the physics of ultra-cold gases in optical lattices. We shall first comment on dipolar BECs in 1D optical lattices, and in particular the role of the non-local inter-site interactions, a major difference between dipolar and non-dipolar gases. We shall then move away from weakly-interacting systems, discussing the extended Hubbard model. This lattice model allows for various quantum phases which are briefly discussed. Finally we shall comment on pair-superfluidity in bilayer Bose systems, and on filament quantum gases in multi-layer systems.

1.3.1 Dipolar BEC in a one-dimensional optical lattice

We shall start our discussion of dipolar gases in optical lattices with the case of a dipolar BEC in a deep one-dimensional optical lattice of the form $V_{latt}(z) = V_0 \sin^2(\pi z/\Delta)$, where Δ is the spacing between two sites of the lattice. For simplicity we shall consider that there is not trapping in the xy-plane.

The potential $V_{latt}(z)$ is a periodic potential, and hence the single-particle energy spectrum is characterised by the appearance of bands and gaps. We shall consider in the following that the gap between the lowest and the second band is large enough compared to other energy scales such that we may reduce our discussion to the lowest band. Since we consider a deep lattice (tight-binding regime), a good basis is provided by the Wannier functions (of the lowest band) $\phi_j(z)$, which are maximally localised at site j. For very deep lattices, $V_{latt}(z)$ may be locally approximated at a site minimum by a harmonic potential, and the corresponding Wannier lattice for the lowest band may be approximated by a Gaussian function. The Wannier functions form a complete set of functions (in the same way as the Bloch functions), and we may then project the BEC wavefunction in the Wannier basis: $\psi(\boldsymbol{r}) = \sum_j \psi_j(\boldsymbol{r}) \equiv \sum_j \Psi_j(x,y)\phi_j(z)$. Employing this projection we may re-write the Hamiltonian in the form

$$\begin{aligned}\hat{H} = &\sum_{j,j'} \left[\int d^3r \psi_j^*(\boldsymbol{r}) \left[\frac{-\hbar^2}{2m}\nabla^2 + V_{latt}(z) \right] \psi_{j'}(\boldsymbol{r}) \right] \\ &+ \frac{1}{2} \sum_{\substack{j,j' \\ l,l'}} \left[\iint d^3r d^3r' \psi_j^*(\boldsymbol{r}) \psi_l^*(\boldsymbol{r}') \psi_{l'}(\boldsymbol{r}') \psi_{j'}(\boldsymbol{r}) U(\boldsymbol{r}-\boldsymbol{r}') \right] \end{aligned} \tag{1.38}$$

where $U(\boldsymbol{r}) = g\delta(\boldsymbol{r}) + U_{dd}(\boldsymbol{r})$.

For sufficiently deep lattices, we may neglect in the first line all terms except for $j = j'$ and those terms where j and j' are nearest neighbours. In the same way we may neglect in the interaction part all terms except those with $j = j'$ and $l = l'$. Due to the Gaussian-like localisation of the on-site wavefunctions $\psi_j(\boldsymbol{r})$, the neglected terms are typically exponentially smaller than the terms kept. The Hamiltonian becomes then of the following form:

$$\begin{aligned}\hat{H} = &-J \sum_{\langle i,j \rangle} \Psi_i^*(\boldsymbol{\rho}) \Psi_j(\boldsymbol{\rho}) + \sum_j \int d^2\boldsymbol{\rho} \Psi_j^*(\boldsymbol{\rho}) \left[\frac{-\hbar^2}{2m}\nabla_{xy}^2 + g\delta_{i,j}\delta(\boldsymbol{\rho}-\boldsymbol{\rho}') \right. \\ &\left. + \int d^2\rho' U_{ij}(\boldsymbol{\rho}-\boldsymbol{\rho}') |\Psi_j(\boldsymbol{\rho}')|^2 \right] \Psi_j(\boldsymbol{\rho}) \end{aligned} \tag{1.39}$$

where

$$J \equiv -\int d^3r \phi_i^*(z) \left[\frac{-\hbar^2}{2m}\partial_z^2 + V_{latt}(z) \right] \phi_j(z), \tag{1.40}$$

$$U_{ij}(\boldsymbol{\rho}-\boldsymbol{\rho}') \equiv \int dz dz' U_{dd}(\boldsymbol{r}-\boldsymbol{r}') |\phi_i(z)|^2 |\phi_j(z')|^2, \tag{1.41}$$

describe, respectively, hopping between nearest neighbours, and the DDI between the site i and the site j. Note that the on-site interactions ($i = j$) result from the interplay

between short-range and dipole-dipole interactions. On the contrary, the inter-site interaction stems directly from the DDI.

Indeed, in non-dipolar gases, inter-site interactions are exponentially suppressed since the range of the interactions is typically much smaller than the inter-site distance. On the contrary, *strong inter-site interactions are a characteristic novel feature introduced by the DDI in the physics of dipolar lattice gases*. In particular, in the case of vanishing hopping ($J = 0$), i.e. in the case of very deep lattices, we would obtain in the case of non-dipolar BECs a set of independent 2D condensates at each layer. Indeed this has been employed in several experiments (Hadzibabic *et al.*, 2006) for achieving 2D gases. On the contrary, the non-local inter-site interaction due to the DDI, makes that the BECs at different layers are not independent, in spite of the absence of hopping.

This has important consequences, for example for the excitations and the stability of dipolar condensates. Let us analyse this.

Dipolar BEC in a single two-dimensional layer. Let us consider first the case of a single layer, i.e. of a quasi-2D dipolar condensate. As mentioned above we can approximate the lattice potential by a harmonic oscillator $V_{latt}(\vec{r}) \simeq m\omega_z^2 z^2/2$. The wavefunction along z may be approximated by a Gaussian $\phi(z) = \exp(-z^2/2l_z^2)/\pi^{1/4}l_z^{1/2}$ ($l_z = \sqrt{\hbar/m\omega_z}$). The effective oscillator length l_z is related to the lattice constant Δ as $l_z \approx \Delta(V_0/E_r)^{-1/4}/\pi$, where $E_r = \hbar^2\pi^2/2m\Delta^2$ is the so-called recoil energy. The ground state of the homogeneous 2D BEC is of the form $\Psi_\perp(\vec{\rho}, t) = \exp(-i(\mu/\hbar + \omega_z)t)\sqrt{n_0}$, where n_0 is the 2D density, and μ is the 2D chemical potential. Introducing this form into the nonlocal GPE, one obtains $\mu = (g + g_d)n_0/\sqrt{2\pi}l_z$. Note that the 2D condition is satisfied for $\mu \ll \hbar\omega_z$.

We may now evaluate the excitation spectrum following the same Bogoliubov-de Gennes procedure employed in previous sections. We insert a plane-wave Ansatz

$$\Psi(\vec{r}, t) = \Phi_0(z)\exp(-i(\mu/\hbar + \omega_z)t) \\ (\sqrt{n_0} + u_q\exp(i\vec{q}\cdot\vec{\rho} - i\epsilon t/\hbar) - v_q^*\exp(-i\vec{q}\cdot\vec{\rho} + i\epsilon t/\hbar)) \tag{1.42}$$

into the GPE, and linearise in u_q, v_q, obtaining the Bogoliubov spectrum:

$$\epsilon(q) = \left\{\frac{\hbar^2 q^2}{2m}\left[\frac{\hbar^2 q^2}{2m} + 2A\right]\right\}^{1/2} \tag{1.43}$$

where $A = \mu - \tilde{g}_d F(ql_z/\sqrt{2})$, with $\tilde{g}_d = g_d n_0/\sqrt{2\pi}l_z$, and $F(x) = \frac{3\sqrt{\pi}}{2}|x|\mathrm{erfc}(x)e^{x^2}$. Note that without DDI ($\beta = 0$) we recover the usual Bogoliubov spectrum for a non-dipolar 2D BEC. In the following we consider $a < 0$ (this is because we would like to have the possibility of a roton-like minimum in the quasi-2D Bogoliubov spectrum, but of course inter-site effects are also remarkable even if $a > 0$). If $a < 0$ and $\beta = 0$, $\epsilon(q)^2 < 0$ for $q \to 0$, recovering the phonon instability in homogeneous BEC with $a < 0$. If the dipole is sufficiently large, such that $g + g_d > 0$, then the DDI prevents the instability at $q \to 0$. However, due to the q-dependence of the DDI (given by the monotonously increasing character of the function F), the dispersion $\epsilon(q)$ may show for intermediate g_d values a roton-like minimum at a finite value of ql_z (this is similar

as in Sec. 1.2.5). For sufficiently low DDI $\epsilon(q)^2 < 0$ at the roton-like minimum, leading to the roton-like instability. For $|\beta| > \beta_{cr}$ (with β_{cr} dependent on the ratio $gn_0/l_z\hbar\omega_z$) roton instability is prevented, and the 2D homogeneous BEC is stable.

Two layers. Let us consider now the case of two layers with no hopping. The system is then described by two coupled GPEs of the form:

$$i\hbar\frac{\partial}{\partial t}\Psi_i(\boldsymbol{\rho},t) = \Bigg[-\frac{\hbar^2}{2m}\nabla^2 + g|\Psi_i(\boldsymbol{\rho},t)|^2 + \sum_j \int d^3r' U_{ij}(\boldsymbol{\rho}-\boldsymbol{\rho}')|\Psi_j(\boldsymbol{\rho}',t)|^2\Bigg]\Psi(\vec{r},t), \tag{1.44}$$

where $i,j = 1,2$. Note that, crucially, the DDI couples now the i-th layer to the j-th one. Similar to the single-site discussion, we consider a strong z-confinement at each site, and hence we may employ a quasi-2D Ansatz $\Psi_i(\vec{r}) = \Psi_{\perp,i}(\vec{\rho},t)\phi(z-z_i)$, where $\phi(z)$ has the form discussed above, and z_i is the position of the i-th lattice node. The ground-state of the condensates at the two layers is given by $\Psi_j = \sqrt{n_0}$. Introducing this Ansatz into the NLSE (1.44) we obtain the 2D chemical potential $\tilde{\mu} = \mu + \lambda(\Delta)$, with μ the chemical potential of an individual well and $\lambda(\Delta) = (g_d n_0/\sqrt{2\pi}l_z)e^{-\Delta^2/2l_z^2}$. Note that the inter-site interaction is a Gaussian function of the inter-site spacing and not of the form $1/\Delta^3$. The Gaussian dependence appears since the inter-site interactions are actually between two planes with an extension much larger (in our homogeneous approximation infinitely larger) than the inter-site distance.

As above we are interested in the elementary excitation of these systems. For $\Delta \to \infty$ the Bogoliubov modes at each site are independent and described by the single-site expression (1.43). For finite Δ the inter-site coupling leads to an hybridisation of the modes at both sites with significant consequences, as we discuss below. As for the single-site discussion we insert a plane-wave Ansatz $\Psi_i(\vec{r},t) = (\sqrt{n_0} + u_{qi}\exp(i\vec{q}\cdot\vec{\rho} - i\epsilon t/\hbar) - v_{qi}^*\exp(-i\vec{q}\cdot\vec{\rho} + i\epsilon t/\hbar))\Phi_0(z-z_i)\exp(-i(\tilde{\mu}/\hbar+\omega_z)t)$ into the NLSE (1.44), and linearise in u_{qi}, v_{qi}. In this way we obtain four coupled Bogoliubov-de Gennes equations for $\{u_{1,2}, v_{1,2}\}$, which may be diagonalised to obtain the Bogoliubov modes:

$$\epsilon_\pm(q) = \left\{E_q\left[E_q + 2A \pm 2C(\Delta)\right]\right\}^{1/2}, \tag{1.45}$$

where

$$C(\Delta) = \lambda(\Delta) - \tilde{g}_d\tilde{F}\left(\frac{ql_z}{\sqrt{2}}, \frac{\Delta}{\sqrt{2}l_z}\right), \tag{1.46}$$

with $\tilde{F}(x,y) = \frac{3\sqrt{\pi}xe^{x^2}}{4}\sum_{\alpha=\pm1} e^{-2\alpha xy}\mathrm{erfc}(x-\alpha y)$.

Note that for $\Delta \to \infty$, $C(\Delta) = 0$ and we recover two degenerate independent modes. For finite Δ the modes at the two wells hybridise, and two different branches appear for each q, one stiffer than the modes for $\Delta \to \infty$, and the other softer. The latter is particularly interesting, since the soft mode is more prone to rotonisation (Fig. 1.10). Interestingly, under proper conditions, two parallel non-overlapping BECs may become roton-unstable even if they were stable separately. As a consequence, a larger β_{cr} is necessary to stabilise the two-well system.

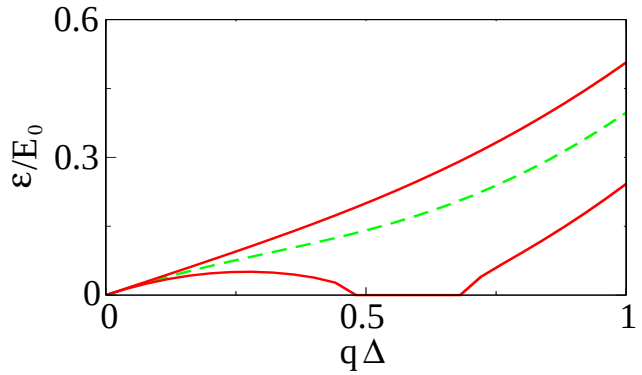

Fig. 1.10 Dispersion law (in units of $E_0 = \hbar^2/m\Delta^2$) for a single site (dashed) and for two wells (solid) for $\beta = -1.2$, $\Delta = 0.53$ μm, $s = 13.3$, $a = -2$ nm, and $n_0/\sqrt{2\pi}l_z = 10^{14}/\text{cm}^3$. See Ref. (Klawunn and Santos, 2009) for details.

Multi-layer case. The hybridisation (and consequent destabilisation) in two-well potentials becomes even more pronounced for the case of dipolar BECs at $N_s > 2$ sites of a 1D optical lattice, since a site i couples with all its neighbours j (of course with decreasing strength for growing $|i-j|$). For simplicity of our analysis we consider the case in which all lattice sites present the same 2D density n_0. In that case, one may easily generalise the two-site analysis to the multi-site case, to reach a set of coupled Bogoliubov-de Gennes equation:

$$\epsilon^2 f_{qi} = E_q(E_q + 2A)f_{qi} + 2E_q \sum_{j\neq i} C(\Delta|i-j|)f_{qj}, \tag{1.47}$$

where $f_{qi} = u_{qi} + v_{qi}$ After diagonalising the matrix of coefficients at the rhs of Eqs. (1.47), one may obtain numerically the corresponding band-like set of N_s elementary excitations (Fig. 1.11). Note that the band-like spectrum has an upper phonon-like boundary which for large N_s has an approximate sound velocity $c_s \simeq \sqrt{(A + \sum_n C(\Delta|n|))/m}$. The lower mode of the N_s manifold becomes significantly softer than the individual modes for independent sites. As a consequence the roton instability extends to larger β_{cr} when N_s increases, until saturating for a sufficiently large N_s (due to the decreasing DDI for increasing distance between sites).

Fig. 1.12 summarises the behaviour of the stability as a function of β (we recall that $g < 0$). As mentioned above if $g + g_d < 0$ ($|\beta| < 1$) the system is unstable against phonon instability. For $1 < |\beta| < |\beta_{cr}(N_s)|$ the system is unstable against roton instability. $|\beta_{cr}|$ increases when N_s grows until saturating for sufficiently large N_s. For $|\beta| > |\beta_{cr}(N_s)|$ the quasi-2D BECs are stable.

Summarising this section, we have seen that interlayer interactions may have rather dramatic effects in dipolar BECs even in the absence of hopping. On one side, the system presents band-like excitations collectively shared by the BECs at different layers. On the other side, a BEC which would be stable in a single layer may become unstable if other layers are present!

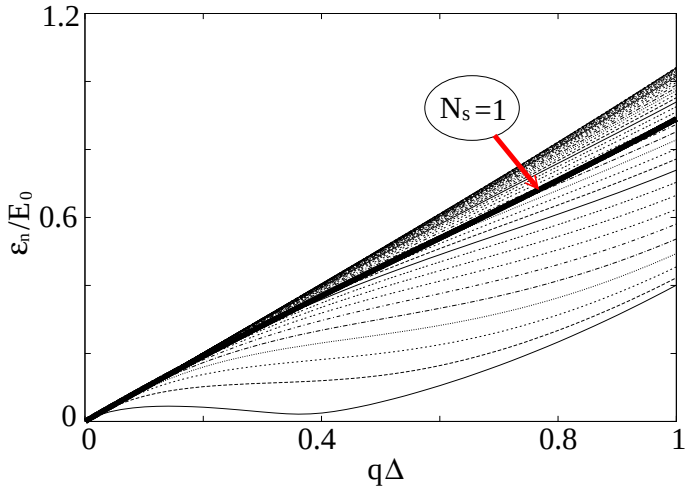

Fig. 1.11 Band-like dispersion (in units of $E_0 = \hbar^2/m\Delta^2$) for $N_s = 40$, $\beta = -2.44$, $\Delta = 0.53$ μm, $s = 13.3$, $a = -2$ nm, and $n_0/\sqrt{2\pi}l_z = 10^{14}/\text{cm}^3$. The dispersion law for $N_s = 1$ is indicated. See Ref. (Klawunn and Santos, 2009) for details.

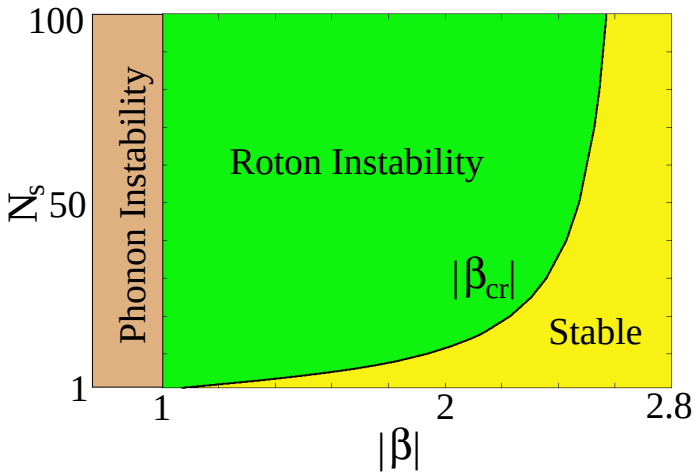

Fig. 1.12 Stable and unstable regimes for N_s dipolar 2D BECs. Same parameters as in Fig. 1.11. See Ref. (Klawunn and Santos, 2009) for details.

1.3.2 Dipole-dipole interactions in strongly-correlated lattice gases: extended Hubbard model

In the previous section we have seen that the inter-site interactions may have quite dramatic effects in the physics of BECs in deep lattices. The DDI may change as well quite significantly the physics of strongly-correlated gases in optical lattices. In this section we shall briefly comment on that.

Let us consider a collection of dipolar bosons loaded in a 2D square lattice $V_{latt}(x, y)$ (fermions will have also an interesting physics but we shall focus here only on bosons). In the transversal direction we assume an harmonic confinement with frequency ω_z,

which is tight enough such that the z wavefunction is the ground-state of the harmonic oscillator $\varphi_0(z)$. We shall assume that the dipoles are oriented perpendicularly to the lattice.

The system is described by the Hamiltonian (note that now we keep the operator character of the fields since we are interested in strongly-correlated systems):

$$\hat{H} = \int d^3r \hat{\psi}^\dagger(\boldsymbol{r}) \left[\frac{-\hbar^2}{2m}\nabla^2 + V_{latt}(x,y) + \frac{1}{2}m\omega_z z^2 + \frac{1}{2}\int d^3r' U(\boldsymbol{r}-\boldsymbol{r}')\hat{\psi}^\dagger(\boldsymbol{r}')\hat{\psi}(\boldsymbol{r}') \right] \hat{\psi}(\boldsymbol{r}), \tag{1.48}$$

where $U(\boldsymbol{r}) = g\delta(\boldsymbol{r}) + U_{dd}(\boldsymbol{r})$, and $\hat{\psi}(\boldsymbol{r})$ is the field operator that annihilates a boson in $\boldsymbol{r}$. As in the discussion of the previous section, since V_{latt} is a periodic potential, the single-particle energy spectrum is characterised by the appearance of bands and gaps. As we did previously, we consider again that we can reduce to the lowest band, and project in the basis of Wannier functions $\Phi_j(\boldsymbol{r})$, which are maximally localised at site j (for a 2D square lattice $j \equiv (j_x, j_y)$). We may then express the field operator as $\hat{\psi}(\boldsymbol{r}) = \sum_j \phi_j(\boldsymbol{r})\hat{a}_j$, where $\phi_j = \Phi_j(x,y)\varphi_0(z)$ and $\hat{a}_j$ annihilates a particle at site j. Employing this projection we may re-write the Hamiltonian in the form

$$\begin{aligned}\hat{H} = &\sum_{j,j'} \left[\int d^3r \phi_j^*(\boldsymbol{r}) \left[\frac{-\hbar^2}{2m}\nabla^2 + V_{latt}(\boldsymbol{r}) \right] \phi_{j'}(\boldsymbol{r}) \right] \hat{a}_j^\dagger \hat{a}_{j'} \\ &+ \frac{1}{2}\sum_{\substack{j,j'\\l,l'}} \left[\iint d^3r d^3r' \phi_j^*(\boldsymbol{r})\phi_l^*(\boldsymbol{r}')\phi_{l'}(\boldsymbol{r}')\phi_{j'}(\boldsymbol{r})U(\boldsymbol{r}-\boldsymbol{r}') \right] \hat{a}_j^\dagger \hat{a}_l^\dagger \hat{a}_{l'}\hat{a}_{j'}\end{aligned} \tag{1.49}$$

We proceed now as in the previous section. For sufficiently deep lattices, we neglect in the first line all terms except for $j = j'$ (this term just leads to a global energy shift of the sites and will be neglected below) and those terms where j and j' are nearest neighbours. In the same way we may neglect in the interaction part all terms except those with $j = j'$ and $l = l'$. We may then reduce the Hamiltonian to the so-called extended Bose-Hubbard model:

$$\hat{H} = -t\sum_{\langle j,j'\rangle} \hat{a}_j^\dagger \hat{a}_{j'} + \frac{U_0}{2}\sum_{j,j'} \hat{n}_j(\hat{n}_j - 1) + \sum_{\substack{\delta\\|\delta|>0}} \frac{U_\delta}{2}\sum_j \hat{n}_j\hat{n}_{j+\delta}, \tag{1.50}$$

where

$$t \equiv -\int d^3r \phi_j^*(\boldsymbol{r}) \left[\frac{-\hbar^2}{2m}\nabla^2 + V_{latt}(\boldsymbol{r}) \right] \phi_{j'}(\boldsymbol{r}), \tag{1.51}$$

$$U_0 \equiv g\int d^3r |\phi_j(\boldsymbol{r})|^4 + \iint d^3r d^3r' |\phi_j(\boldsymbol{r}')|^2 |\phi_j(\boldsymbol{r})|^2 U(\boldsymbol{r}-\boldsymbol{r}'), \tag{1.52}$$

$$U_\delta \equiv \iint d^3r d^3r' |\phi_j(\boldsymbol{r}')|^2 |\phi_{j+\delta}(\boldsymbol{r})|^2 U(\boldsymbol{r}-\boldsymbol{r}'), \tag{1.53}$$

$$\tag{1.54}$$

describe, respectively, hopping between nearest neighbours, on-site interactions, and inter-site interactions. As in our discussion of Sec. 1.3.1, note again that, crucially, the on-site interactions $U_0 \equiv U_0^{(sc)} + U_0^{(dd)}$ result from the interplay between short-range ($U_0^{(sc)}$) and dipole-dipole interactions ($U_0^{(dd)}$), but the inter-site interaction (U_δ) stems directly from the DDI. Hence the possibly quite strong interactions between sites are a novel effect introduced by the DDI, which may change radically the physics of strongly-correlated gases in optical lattices, as we shall discuss below.

Note that dipolar gases in 2D lattices allow for different forms of control of the couplings constants of the extended Hubbard Hamiltonian:

- As for any other lattice gases, we may change the hopping t by changing the depth of the lattice.
- Again, as for any lattice gas we may change the short-range interactions by employing Feshbach resonances. Note that this will affect the on-site interactions (U_0).
- Note that due to the anisotropy of the DDI the spatial dependence of the on-site wavefunction may significantly modify $U_0^{(dd)}$. In particular, depending on the relation between the transversal oscillator length and the on-site extension in the xy plane, $U_0^{(dd)}$ may be positive or negative. Hence, remarkably, by controlling the geometry of the trapping we may control $U_0^{(dd)}$, allowing for the change between different interaction regimes. For example, we may reach the situation in which $U_0 = 0$ although $U_\delta \neq 0$, i.e. we may get an extended Hubbard model without on-site interactions!
- Note also that the U_δ coupling constants decay with δ (for zero-dimensional sites as $1/\delta^3$). As a consequence it depends on the dipole strength and the lattice constant whether U_δ is relevant (compared to other energy scales in the system, in particular the on-site interaction U_0). Under some conditions one may consider just the nearest neighbour (U_1) or the next-to-nearest neighbour (U_2), but for a strong dipole (as that of very polar molecules) even further neighbours contribute significantly.
- Although we do not use it here, we may also modify the angle between the vector normal to the lattice and the dipole direction. In that case, the inter-site interactions would be anisotropic on the 2D lattice.

Hence, in addition to standard control possibilities, dipolar gases offer novel possibilities for the control of quantum gases in optical lattices.

1.3.3 Quantum phases of dipolar bosons in optical lattices

For the case $U_\delta = 0$ (i.e. the non-dipolar case) we recover the usual Bose-Hubbard model. It is quite well known that in that case, and depending on the chemical potential, the tunneling and the on-site interactions the system may present two distinct quantum phases: a superfluid phase, and a Mott-insulator phase (with a commensurate filling per site). In dipolar gases, the extended Hubbard model leads to a much richer physics of possible quantum phases, which we can only barely discuss here. Let us briefly discuss some of the most remarkable consequences.

Supersolid. Since the dipole is perpendicular to the lattice plane $U_\delta > 0$, i.e. we have repulsive inter-site interactions. As a result, it seems quite intuitive that the bosons will "dislike" to be at neighbouring sites, and hence it is not surprising that for strong enough interactions the density of particles may present a modulation (which is not the trivial modulation induced by the lattice). Actually for a sufficiently large U_δ (and a commensurate filling $\bar{n} = 1/2$) the system may enter into a checkerboard phase (Góral *et al.*, 2002), i.e. the bosons are placed like in the dark squares of a checkerboard. This phase is obviously an insulating phase (and actually one may call it a Mott insulator with half-filling).

However, a much more intriguing phase may occur (Góral *et al.*, 2002), in which the system remains superfluid but the density presents a modulation. This phase is called a supersolid, and constitute one of the holy grails of condensed-matter physics. In principle this phase may be unstable against phase separation into an insulating crystal and a superfluid. It has been recently shown by means of Quantum Monte Carlo calculations that a supersolid may be stabilised against phase separation in an extended Bose-Hubbard model with just nearest neighbour interactions, as long as the filling of the lattice $\bar{n} > 1/2$ and $U_1 > U_0/z$ (where z is the coordination number of the lattice, $z = 4$ for a square lattice) (Sengupta *et al.*, 2005). Note that as mentioned above we may easily control the ration U_1/U_0 by Feshbach resonances or by modifying the transversal confinement, and hence the supersolid phase may be stabilised. Not only a checkerboard supersolid is possible, but also under proper circumstances (e.g. including next-to-nearest neighbour interactions) one may achieve supersolids with other patterns (striped and quarter-filled crystals) (Chen *et al.*, 2008).

Haldane insulator. Another interesting phase induced by the DDI has been discussed for the case of bosonic dipoles in a 1D optical lattice by Dalla Torre et al. (Dalla Torre *et al.*, 2006). Let us consider the case of a filling factor $\bar{n} = 1$ per site. Let us assume that we may have sites with zero particles but consequently also sites with $n = 2$. Let us assume that only these three possibilities are possible $n = 0, 1, 2$. One may cut at $n = 2$ if U_0 is sufficiently large, however one may check that the presence of sites with $n = 3$ does not spoil the physics discussed below. We may then introduce a pseudo-spin $S_z = n - \bar{n}$, which may acquire values $-1, 0, 1$. Hence, interestingly, the system is to a large extent equivalent to a spin-1 gas system with extended interactions, realizing a so-called Haldane spin-1 chain. It is known that such system may present a rather intriguing phase characterised by string correlations which imply that $S_z = \pm 1$ appear in alternating order along the chain separated by strings of $S_z = 0$ of arbitrary length. In other words, we have a site with zero (two) particles, followed by whatever number of sites with one particle, and then we have a site with two (zero) particles. So something like:

$$\ldots 1\,\mathbf{0}\,1\ldots 1\,\mathbf{2}\,1\ldots 1\,\mathbf{0}\,1\ldots 1\,\mathbf{2}\,1\ldots$$

This phase is characterised by

$$\langle \delta n_i e^{i\pi \sum_{k=i}^{j} \delta n_k} \delta n_j \rangle \to \text{const} \neq 0. \tag{1.55}$$

In Ref. (Dalla Torre *et al.*, 2006) it has been shown that this rather subtle phase may be probed by parametrically modulating the lattice, and having a look into the

absorption rate associated to the linear response (a delta like peak appears in the absorption spectrum).

Metastable states. In addition to the ground-state phases discussed above (and some other more exotic which we shall not discuss) the DDI lead to another interesting phenomenon, namely the proliferation of metastable states, characterised by a non-uniform particle distribution in the lattice (Menotti *et al.*, 2007). These states correspond to local energy minima with a very long life time. The existence of these metastable states may be understood from the competing length scales in the problem, i.e. the combination of different non-local interactions at different neighbours. As a result, disordered configurations of atoms lead to a disorder self-induced interaction potential. This self-induced disorder resembles to a large extent the so-called structural glasses in condensed-matter physics (Schmalian and Wolynes, 2000).

Because of the presence of those very many metastable states, in an experiment it may be hard to reach the ground state or a given metastable configuration. One can use however super-lattices in order to prepare the atoms in configurations of preferential symmetry. Note that the configurations obtained in such a way will also remain stable once the super-lattice is removed, thanks to the DDI.

1.3.4 Pair superfluidity in bilayer systems

Up to now we have considered the case of a 2D lattice gas of polar molecules. A very interesting physics may appear if we have more than one such 2D layers. As mentioned in Sec. 1.3.1 for the case of BECs, this is true even if there is no hopping between layers. We shall illustrate this by having first a look to the idea of pair superfluidity in bilayer systems. In the next section we shall comment on how DDI may lead to filament quantum gases in multi-layers.

In the following, we consider dipolar bosons placed at two neighbouring, but disconnected, 1D traps (wires). Along the 1D systems we assume an additional lattice equal for both 1D traps, We have hence a ladder-like configuration. In order to illustrate clearly the effects of inter-layer interactions we consider a configuration for which only the (attractive) dipole-dipole interaction between sites at the same rung plays a significant role. This is physically possible for particular 1D dipole configurations (see (Argüelles and Santos, 2007) for details), but here we just assume it for simplicity of the discussion. Of course, in general the (repulsive) DDI between sites belonging to the same wire cannot be neglected, and interesting physics will result from there, as we shall briefly mention below.

Under the previous conditions the system is described by a Bose-Hubbard Hamiltonian similar to that of Eq. 1.50, but now with two wires

$$\hat{H} = -J \sum_{\alpha=1,2} \sum_{<i,j>} \{\hat{b}_i^{(\alpha)\dagger} \hat{b}_j^{(\alpha)} + H.c.\} - \mu \sum_{\alpha=1,2} \hat{n}_i^{(\alpha)}$$
$$+ \frac{U_0}{2} \sum_{\alpha=1,2} \sum_i \hat{n}_i^{(\alpha)} (\hat{n}_i^{(\alpha)} - 1) - |U'| \sum_i \hat{n}_i^{(1)} \hat{n}_i^{(2)}, \tag{1.56}$$

where $\hat{b}_i^{(\alpha)}$, $\hat{b}_i^{(\alpha)\dagger}$, and $\hat{n}_i^{(\alpha)}$ are, respectively, the annihilation, creation, and number operators for the site i at the wire α. J describes the hopping between neighbouring

sites i and j in each wire, U_0 the on-site interactions (as already mentioned this is a combination of short-range and dipolar contributions), and we consider the same chemical potential μ in both wires. Atoms in sites at the same rung interact attractively by the DDI, which is characterised by a coupling $-|U'|$.

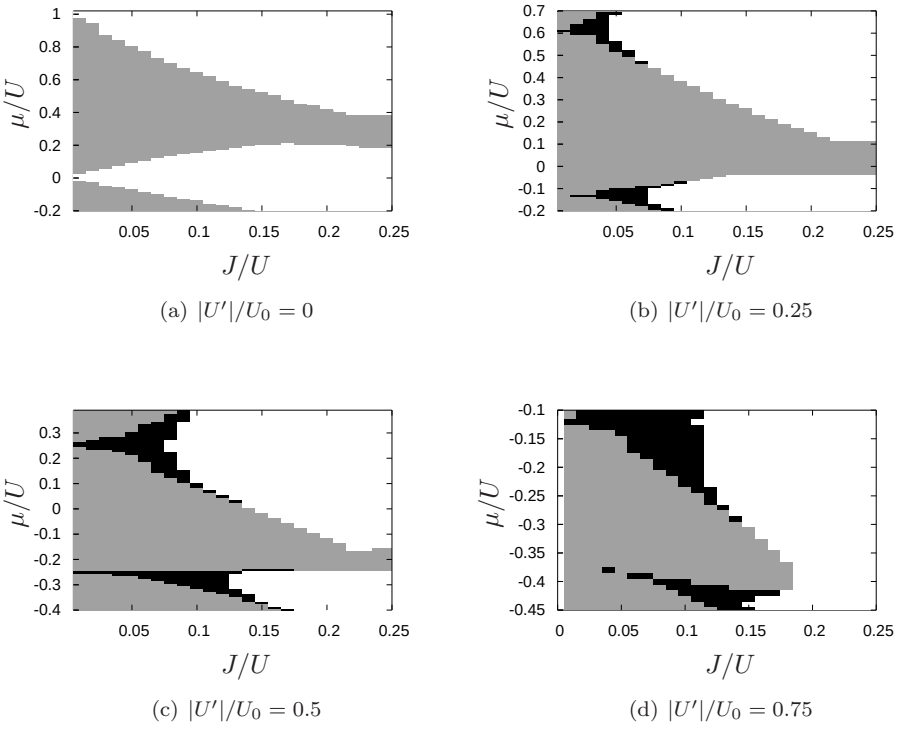

(a) $|U'|/U_0 = 0$

(b) $|U'|/U_0 = 0.25$

(c) $|U'|/U_0 = 0.5$

(d) $|U'|/U_0 = 0.75$

Fig. 1.13 Phase diagram for $|U'|/U_0 = 0$ (a), 0.25 (b), 0.5 (c), and 0.75(d), where white represents 2SF, gray MI, and black PSF. Figure from Ref. (Argüelles and Santos, 2007)(E).

The ground-state phases are characterised by the correlation functions $G_1(\Delta) = \langle \hat{b}^\dagger_{0,\alpha} \hat{b}_{\Delta,\alpha} \rangle$ and $G_2(\Delta) = \langle \hat{b}^\dagger_{0,1} \hat{b}^\dagger_{0,2} \hat{b}_{\Delta,1} \hat{b}_{\Delta,2} \rangle$. Note that G_1 is the single-particle density matrix along an individual wire, whereas G_2 is related with pairs placed in the same rung of the ladder but at opposite wires. The phase diagram of the system presents three distinct phases (Fig. 1.13):

- Mott-insulator (MI) (shaded regions): this is characterised by a commensurate occupation at the sites of both wires. Figure 1.13 shows DMRG results for the surroundings of the lowest MI lobe (with occupation $\langle n_i^\alpha \rangle = 1$) for $|U'|/U_0 = 0$ (a), 1/4 (b), 1/2 (c) and 3/4 (d). Note that in order to avoid collapse in a single site, $|U'| < U_0$. For the case of $U' = 0$, the usual Mott-lobes (shaded regions) are recovered. This is an insulating region, in which both correlations G_1 and G_2

decay exponentially.

- Pair-superfluid (PSF) (black regions). In this phase G_1 still decays exponentially but G_2 decays polynomically. We have hence a superfluid phase, but the superfluidity is given by the formation of pairs.
- Two-superfluid phase (2SF) (white regions). In this phase both G_1 and G_2 decay polynomically.

The MI and 2SF phases correspond to the usual MI and SF phases known for the Bose-Hubbard Hamiltonian. The PSF phase in bilayer systems is however rather peculiar for dipolar gases, resembling the situation known for two-component Bose gases (Kuklov *et al.*, 2004).

Actually, the presence of the PSF phase drastically modifies the MI lobes (Fig. 1.13). Let us briefly comment why this is so. The boundaries of the MI lobes are provided by the energy gap between the MI state and the lowest excited state conserving the particle number. In an usual Bose-Hubbard Hamiltonian (one wire, local interactions) (Fisher *et al.*, 1989) this lowest excitation is provided by particle-hole excitations. The MI boundaries can then be calculated by a strong-coupling expansion (SCE) (Freericks and Monien, 1996), estimating the energy of a state with an extra particle and a state with an extra hole. This is indeed the case of $U' = 0$, where the lowest excitations are given by uncorrelated particle-hole excitations in both wires. The situation changes for $|U'| > 0$, since for sufficiently low tunneling, there is a direct transition between MI and PSF phases, i.e. superfluid phases of composites (or composite holes). In that case the first excitation of the MI lobe is given by the correlated creation of pairs of particles (or holes) at opposite sites of the two wires, explaining the qualitative change in the shape of the lobe boundaries. In particular, a second-order SCE in $J/|U'|$, provides the following dependence for sufficiently low tunneling for the lowest boundary of the MI lobe with n_0 particles per site:

$$\frac{\mu}{U_0} = n_0 - 1 + \frac{|U'|}{U_0}\left(\frac{1}{2} - n_0\right) \\ -4\left(\frac{J}{U_0}\right)^2\left[n_0(n_0+1) - \frac{(n_0^2-1)/2}{2-|U'|/U_0} - \frac{n_0^2 U_0}{|U'|}\right] \tag{1.57}$$

From Eq. (1.57) it becomes clear that for any $U' > 0$ the gap boundaries are quadratic (and not linear) in J for sufficiently low J (this is of course so because the motion goes in pairs). Interestingly, the lowest boundary of the first MI region ($n_0 = 1$) inverts its slope at $J = 0$ for $|U|' > U_0/2$, in agreement with our numerical results. One may also observe that an inversion of the slope of the lowest boundary is expected also for $n_0 = 2$ at $|U'|/U_0 \simeq 0.85$, but it is not expected for $n_0 > 2$.

The reentrant shape of the MI lobes leads to a non-trivial behaviour of the MI plateaux (wedding-cake structure) in experiments with an axial harmonic confinement. In particular, the MI plateaux may (for low hopping) become insensitive to the hopping, or even counter-intuitively grow for larger tunneling. Actually this result may be extended to 2D lattices at unconnected layers where the first MI lobe follows at low J the relation (1.57) but substituting $2(J/U_0)^2$ by $z(J/U_0)^2$, where z is the coordination number.

To finish this section let us point that if the repulsion along the wires (or within the layers in 2D) is considered the bending of the Mott-lobes is preserved, and a pair-supersolid phase may be obtained (Trefzger *et al.*, 2009). In addition, the presence of inter-layer hopping may lead also to interesting effects (see e.g. (Wang, 2007)). We would also like to note that a series of very recent works have analysed the related case of polar Fermi molecules in bilayer systems when the electric dipoles are oriented perpendicular to the layer planes, and the inter-layer hopping is negligible. This situation is particularly interesting for current experiments in JILA, since chemical recombination may be strongly reduced in 2D configurations (Ni *et al.*, 2010), as it will be the case for the different layers. The interlayer interaction is attractive and may allow for interlayer superfluidity, and the equivalent of a BCS-BEC crossover (Potter *et al.*, 2010; Klawunn *et al.*, 2010*b*; Pikovski *et al.*, 2010; Baranov *et al.*, 2010).

1.3.5 Quantum filament gases in multi-layer systems

In the previous section we saw that the interlayer interactions may lead to the formation of interlayer superfluidity given by pairs of particles placed at opposite layers. Interestingly, it is clear that similar reasonings suggest that filaments may be formed in multi-layer systems. These filaments may present a very interesting physics which is only very partially understood. For simplicity of the discussion we shall have a look here to possibly the simplest scenario which already contains many of the ingredients which could make filament quantum gases so interesting. We consider polar Fermi molecules in a three-layer system (actually for this discussion we shall consider three quasi-1D wires), without inter-wire hopping, and with an harmonic trapping along the wire. We shall consider the attractive interaction between dipoles at different wires, but neglect interactions between dipoles along the wires. This is of course a rather rough approximation, although in 1D it may be the case under proper conditions (Klawunn *et al.*, 2010*a*). In general intra-layer interactions will play an important role, but at least part of the physics discussed here will be qualitatively maintained. Polar bosonic molecules in multi-layers (under similar approximations as those discussed here) were considered by Wang et al. (Wang *et al.*, 2006) (see comment below).

The attraction between polar molecules placed on top of each other may be strong-enough to bind two or more polar molecules into self-assembled chains (Fig. 1.14). Whereas for bosonic molecules these chains are in any case bosons (Wang *et al.*, 2006), for fermionic molecules the fermionic/bosonic character of the filaments depends on the odd/even number of molecules in a given chain. In particular, the three-well configuration allows for fermionic trimers (and of course monomers), and two different kinds of bosonic dimers, namely those between two molecules at nearest neighbours (type I dimers), and those between two molecules at the uppest and lowest site (type II dimers) (Fig. 1.14). Note that dimers I are actually pseudo-spin-1/2 bosons, since dimers in sites 1 and 2 are not equivalent to dimers in sites 2 and 3.

In addition, it is important to note that transverse filament excitations contribute to the gas entropy, being relevant at finite temperature T. These modes are string-like perturbations of the straight filaments. Contrary to the case of bosonic molecules (Wang *et al.*, 2006), transverse modes are important for fermionic molecules even at very low T since they may significantly reduce the trimer Fermi energy.

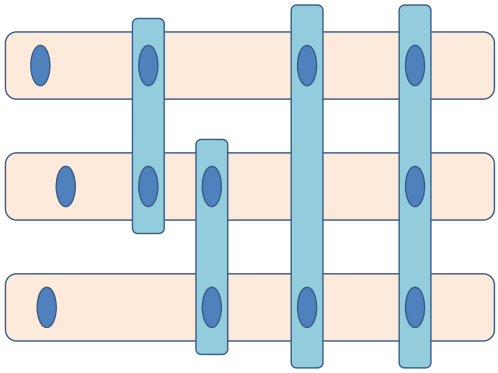

Fig. 1.14 Polar fermionic molecules in a three-well potential may remain unpaired, form fermionic trimers, or bosonic dimers between nearest neighbours or next-nearest neighbours.

In the following we consider the filament statistics, assuming an ideal filament gas. This rough approximation largely simplifies the analysis of the problem, while allowing for the discussion of key qualitative features of these systems, in particular the competition between different Bose and Fermi composites. The fermionic or bosonic character of the chains is reflected by the average occupations for trimers, dimers I, dimers II and monomers:

$$N_T(n,\nu_T) = \left[e^{\beta[-E_T+\xi_{\nu_T}+\epsilon_n-(2\mu_1+\mu_2)]}+1\right]^{-1} \tag{1.58}$$

$$N_{D,I}(n,\nu_{D,I}) = \left[e^{\beta[-E_{D,I}+\xi_{\nu_{D,I}}+\epsilon_n-(\mu_1+\mu_2)]}-1\right]^{-1} \tag{1.59}$$

$$N_{D,II}(n,\nu_{D,II}) = \left[e^{\beta[-E_{D,II}+\xi_{\nu_{D,II}}+\epsilon_n-2\mu_1]}-1\right]^{-1} \tag{1.60}$$

$$N_{S,j}(n) = \left[e^{\beta[\epsilon_n-\mu_j]}+1\right]^{-1} \tag{1.61}$$

where $N_{S,j}$ denotes the average occupation of individual molecules at wire j, $-E_T$, $-E_{D,I}$ and $-E_{D,II}$ are the binding energies for, respectively, trimers, dimers I, and dimers II, $\xi_{\nu_{T;D,I;D,II}}$ are the transverse filaments modes of the different composites, $\epsilon_n = \hbar\omega(n+1/2)$ are the harmonic oscillator levels of the trap along the wires, and $\beta = 1/k_BT$ the inverse temperature. In the previous expressions we have assumed symmetric configurations such that the number of dimers I in sites 1–2 is the same as the number of dimers I in sites 2–3, and equal to $N_{D,I}(n,\nu_{D,I})$. Note that $\mu_1 = \mu_3$ is the chemical potential for molecules at the uppest and lowest sites, whereas μ_2 denotes the chemical potential for molecules in the middle site. These different chemical potentials are necessary to fulfil the normalisation conditions, in which we assume N molecules per lattice site. Imposing symmetry between the uppest and the lowest sites, these conditions acquire the form:

$$N = N_T + N_{D,I} + N_{D,II} + N_{S,1}, \tag{1.62}$$

$$N = N_T + 2N_{D,I} + N_{S,2}, \tag{1.63}$$

where N_T, $N_{D,I}$, $N_{D,II}$, $N_{S,1}$ and $N_{S,2}$ denote respectively the total number of trimers, dimers I in sites 1–2 (or 2–3), dimers II, monomers in site 1 (or 3) and monomers in

site 2. From (1.62) and (1.63) we obtain $\mu_1(N,T)$ and $\mu_2(N,T)$, and from (1.58–1.61) the occupation numbers.

Due to the attractive DDI between molecules in the filament, the most bound chain is the trimer. The difference in binding between dimers and trimers induces that for sufficiently small N and at low-enough T the DCL becomes a degenerate Fermi gas of trimers. The trimers fill up oscillator levels (and also transverse trimer modes) up to the corresponding Fermi energy $E_F(N)$, which equals $N\hbar\omega$ for rigid filaments but it is actually smaller due to the transverse trimer modes. However, if the number of molecules per site is sufficiently large, the growth in Fermi energy overcomes the binding energy difference. This transition may be easily estimated by comparing the average energy per molecule for the case of two trimers and that for the case of 2 dimers I and one dimer II. This leads to a condition for the critical number of molecules per site $N_c(U_0,\omega)$, $E_F(N_c) = 2E_T - 3(E_{D,I} + E_{D,II})/2$ (which we have confirmed numerically). Note that N_c grows with growing interlayer attraction and decreasing trap frequency ω. For $N < N_c$ the quantum gas is a degenerate trimer gas, whereas for $N > N_c$ the trimer gas coexists with a mixture of pseudo-spin-1/2 bosons (dimers I) and spin-less bosons (dimers II).

The peculiar properties of the DCL translate into the spatial molecular distribution integrated over the three sites. For $N < N_c$ and $N < \xi_{1_T}/\omega$, only trimers in their internal ground state are formed, and hence the gas behaves as a spin-less Fermi gas of particles of mass $3m$, presenting a Thomas-Fermi density profile $(1-(x/R)^2)^{1/2}$ with $R/l_{HO} = \sqrt{2N/3}$. For $\xi_{1_T}/\omega < N < N_c$, the DCL is still a trimer gas, but transversal trimer modes may be populated. In that case the density profile departs from the Thomas-Fermi profile (Fig. 1.15, top), due to the appearance of internally excited trimers in low harmonic oscillator levels. For $N > N_c$ the density profile changes dramatically. Note that since we consider 1D gases, dimer BEC is strictly speaking precluded. However, due to finite size the dimers quasi-condense (at low-enough T) occupying the few lowest levels of the harmonic oscillator. Hence when N surpasses N_c a Bose cloud nucleates at the trap centre. As a result the distribution of the polar molecules shows a Gaussian-like peak at the trap centre (Fig. 1.15, bottom).

For $N \gg N_c$ and $U_0 > U_0^*(D,II)$ the quantum gas is at low T a basically pure Bose gas of dimers I and II (except for a small trimer fraction). Since both dimers have double mass, the difference between them cannot be discerned from the analysis of the integrated density profile of the molecules. However the different binding energy and excited dimer modes for both types of dimers may be studied spectroscopically to reveal the dual nature of the mixture.

The filament gas presents as well an intriguing finite temperature physics due to the role of filament modes and the different binding energy of dimers and trimers. This is particularly clear from a finite T analysis with $N < N_c$. Whereas at very low T the DCL is purely a trimer Fermi gas, at finite T it becomes more favourable to populate dimers than to populate higher excited trimer states. As a consequence the system presents a striking thermal enhancement of the bosonic modes. Interestingly, contrary to the standard situation, this leads to a maximal central peak density for a given finite T. For even larger T the central density decreases again due to the occupation of dimers at higher oscillator modes, and the breaking of the filaments into individual

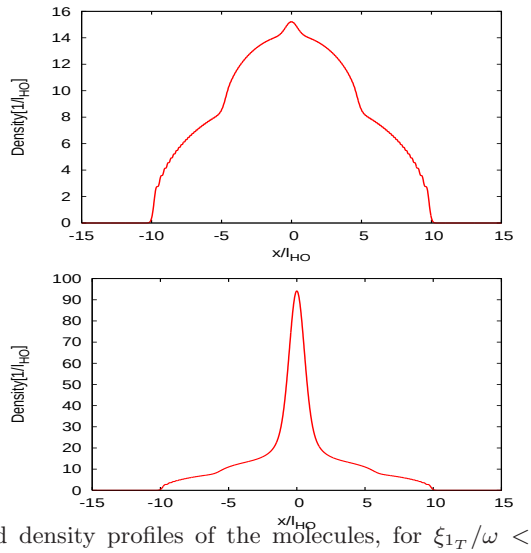

Fig. 1.15 Integrated density profiles of the molecules, for $\xi_{1_T}/\omega < N < N_c$ (top), and $N > N_c$ (bottom). We consider $U_0 = 2$, $\omega/2\pi = 1$Hz, $m = 100$amu, which lead to $N_c = 230$. Figure from Ref. (Klawunn *et al.*, 2010*a*).

molecules.

Let us finally point that for the case of bosonic polar particles, the filaments are obviously always bosonic. As a result, at sufficiently low temperature there is a Bose-Einstein condensation of the largest filaments (which, we recall, are the ones with the tightest binding) (Wang *et al.*, 2006).

Although this simple theory contains very suggestive ingredients, including the possibility of filaments BEC, the competition between fermionic and bosonic filaments, and the role of the transversal modes, it is clear that inter-filament interactions will lead to interesting novel properties, which are still not well understood.

1.4 Conclusions

Since the properties of ultra-cold gases are to a large extent determined by inter-particle interactions, the presence of dipole-dipole interactions in addition to the usual van-der-Waals like interactions introduces qualitative changes in the physics of dipolar gases. In these notes we have reviewed some of this interesting physics, which concern a large variety of areas, ranging from non-linear atom optics to condensed-matter physics. In this sense, although recent experiments on atomic Chromium condensates have already unveiled part of the expected richness of dipolar gases, it is expected that a new generation of experiments on polar molecules (and possibly also Rydberg gases) may soon reach quantum degeneracy opening the path for strongly polar quantum gases. As mentioned in these notes these systems are expected to provide radically new scenarios for ultra-cold gases. One should hence expect exciting developments on dipolar gases in the next future.

References

Argüelles, A. and Santos, L. (2007). *Phys. Rev. A*, **75**, 053613.

Baranov, M. A. (2008). *Physics Reports*, **464**, 71.

Baranov, M. A., Micheli, A., Ronen, S., and Zoller, P. (2010). arXiv:1012.5589.

Beaufils, Q., Chicireanu, R., Zanon, T., Laburthe-Tolra, B., Maréchal, E., Vernac, L., Keller, J.-C., and Gorceix, O. (2008). *Phys. Rev. A*, **77**, 061601.

Bohn, J., Wilson, R., and Ronen, S. (2009). *Laser Physics*, **19**, 547. 10.1134/S1054660X09040021.

Bortolotti, D. C. E., Ronen, S., Bohn, J. L., and Blume, D. (2006). *Phys. Rev. Lett.*, **97**, 160402.

Chen, Y.-C., Melko, R. G., Wessel, S., and Kao, Y.-J. (2008). *Phys. Rev. B*, **77**, 014524.

Cinti, F., Jain, P., Boninsegni, M., Micheli, A., Zoller, P., and Pupillo, G. (2010). *Phys. Rev. Lett.*, **105**, 135301.

Conti, C., Peccianti, M., and Assanto, G. (2003). *Phys. Rev. Lett.*, **91**, 073901.

Dalla Torre, E. G., Berg, E., and Altman, E. (2006). *Phys. Rev. Lett.*, **97**, 260401.

Deb, B. and You, L. (2001). *Phys. Rev. A*, **64**, 022717.

Deiglmayr, J., Grochola, A., Repp, M., Mörtlbauer, K., Glück, C., Lange, J., Dulieu, O., Wester, R., and Weidemüller, M. (2008). *Phys. Rev. Lett.*, **101**, 133004.

Dutta, O. and Meystre, P. (2007). *Phys. Rev. A*, **75**, 053604.

Eberlein, C., Giovanazzi, S., and O'Dell, D. H. J. (2005). *Phys. Rev. A*, **71**, 033618.

Fattori, M., Roati, G., Deissler, B., D'Errico, C., Zaccanti, M., Jona-Lasinio, M., Santos, L., Inguscio, M., and Modugno, G. (2008). *Phys. Rev. Lett.*, **101**, 190405.

Fisher, Matthew P. A., Weichman, Peter B., Grinstein, G., and Fisher, Daniel S. (1989). *Phys. Rev. B*, **40**, 546–570.

Freericks, J. K. and Monien, H. (1996). *Phys. Rev. B*, **53**, 2691–2700.

Gammal, A., Frederico, T., and Tomio, L. (2001). *Phys. Rev. A*, **64**, 055602.

Góral, K. and Santos, L. (2002). *Phys. Rev. A*, **66**, 023613.

Góral, K., Santos, L., and Lewenstein, M. (2002). *Phys. Rev. Lett.*, **88**, 170406.

Griesmaier, A., Stuhler, J., Koch, T., Fattori, M., Pfau, T., and Giovanazzi, S. (2006). *Phys. Rev. Lett.*, **97**, 250402.

Griesmaier, A., Werner, J., Hensler, S., Stuhler, J., and Pfau, T. (2005). *Phys. Rev. Lett.*, **94**, 160401.

Hadzibabic, Z., Kruger, P., Cheneau, M., Battelier, B., and Dalibard, J. (2006). *Nature*, **441**, 1118.

Henkel, N., Nath, R., and Pohl, T. (2010). *Phys. Rev. Lett.*, **104**, 195302.

Ho, T.-L. (1998). *Phys. Rev. Lett.*, **81**, 742–745.

Kawaguchi, Y., Saito, H., and Ueda, M. (2006). *Phys. Rev. Lett.*, **96**, 080405.

Khaykovich, L., Schreck, F., Ferrari, G., Bourdel, T., Cubizolles, J., Carr, L. D.,

Castin, Y., and Salomon, C. (2002). *Science*, **296**(5571), 1290–1293.
Klawunn, M., Duhme, J., and Santos, L. (2010*a*). *Phys. Rev. A*, **81**, 013604.
Klawunn, M., Pikovski, A., and Santos, L. (2010*b*). *Phys. Rev. A*, **82**, 044701.
Klawunn, M. and Santos, L. (2009). *Phys. Rev. A*, **80**, 013611.
Koch, T., Lahaye, T., Metz, J., Frohlich, B., Griesmaier, A., and Pfau, T. (2005). *Nat. Phys.*, **4**, 218.
Komineas, S. and Cooper, N. R. (2007). *Phys. Rev. A*, **75**, 023623.
Kotochigova, S., Julienne, P. S., and Tiesinga, E. (2003). *Phys. Rev. A*, **68**, 022501.
Krolikowski, W., Bang, O., Rasmussen, J. J., and Wyller, J. (2001). *Phys. Rev. E*, **64**, 016612.
Kuklov, A., Prokof'ev, N., and Svistunov, B. (2004). *Phys. Rev. Lett.*, **92**, 050402.
Lahaye, T, C., Menotti, L., Santos, Lewenstein, M., and Pfau, T. (2009). *Reports on Progress in Physics*, **72**, 126401.
Lahaye, T., Metz, J., Fröhlich, B., Koch, T., Meister, M., Griesmaier, A., Pfau, T., Saito, H., Kawaguchi, Y., and Ueda, M. (2008). *Phys. Rev. Lett.*, **101**, 080401.
Landau, L. D. and Lishitz, E. M. (1977). *Quantum Mechanics* (2nd edn). Butterworth-Heinemann, New York.
Litvak, A. G., Mironov, V. A., Fraiman, G. M., and Yunakoskii, A. D. (1975). *Sov. J. Plasma Phys.*, **1**, 60.
Marinescu, M. and You, L. (1998). *Phys. Rev. Lett.*, **81**, 4596–4599.
Menotti, C., Trefzger, C., and Lewenstein, M. (2007). *Phys. Rev. Lett.*, **98**, 235301.
Micheli, A., Pupillo, G., Büchler, H. P., and Zoller, P. (2007). *Phys. Rev. A*, **76**, 043604.
Nath, R., Pedri, P., and Santos, L. (2007). *Phys. Rev. A*, **76**, 013606.
Nath, R., Pedri, P., and Santos, L. (2009). *Phys. Rev. Lett.*, **102**, 050401.
Nath, R. and Santos, L. (2010). *Phys. Rev. A*, **81**, 033626.
Ni, K.-K., Ospelkaus, S., de Miranda, M. H. G., Pe'er, A., Neyenhuis, B., Zirbel, J. J., Kotochigova, S., Julienne, P. S., Jin, D. S., and Ye, J. (2008). *Science*, **322**, 231.
Ni, K.-K., Ospelkaus, S., Wang, D., Quemener, G., Neyenhuis, B., de Miranda, M. H. G., Bohn, J. L., Ye, J., and Jin, D. S. (2010). *Nature*, **464**, 1324.
O'Dell, D. H. J., Giovanazzi, S., and Eberlein, C. (2004). *Phys. Rev. Lett.*, **92**, 250401.
Pasquiou, B., Bismut, G., Maréchal, E., Pedri, P., Vernac, L., Gorceix, O., and Laburthe-Tolra, B. (2011). *Phys. Rev. Lett.*, **106**, 015301.
Pedri, P. and Santos, L. (2005). *Phys. Rev. Lett.*, **95**, 200404.
Pikovski, A., Klawunn, M., Shlyapnikov, G. V., and Santos, L. (2010). *Phys. Rev. Lett.*, **105**, 215302.
Pollack, S. E., Dries, D., Junker, M., Chen, Y. P., Corcovilos, T. A., and Hulet, R. G. (2009). *Phys. Rev. Lett.*, **102**, 090402.
Potter, A. C., Berg, E., Wang, D.-W., Halperin, B. I., and Demler, E. (2010). *Phys. Rev. Lett.*, **105**, 220406.
Ruprecht, P. A., Holland, M. J., Burnett, K., and Edwards, M. (1995). *Phys. Rev. A*, **51**, 4704.
Santos, L. and Pfau, T. (2006). *Phys. Rev. Lett.*, **96**, 190404.
Santos, L., Shlyapnikov, G. V., and Lewenstein, M. (2003). *Phys. Rev. Lett.*, **90**, 250403.

Santos, L., Shlyapnikov, G. V., Zoller, P., and Lewenstein, M. (2000). *Phys. Rev. Lett.*, **85**, 1791–1794.
Schmalian, J. and Wolynes, P. G. (2000). *Phys. Rev. Lett.*, **85**, 836–839.
Schmidt, P. O., Hensler, S., Werner, J., Griesmaier, A., Görlitz, A., Pfau, T., and Simoni, A. (2003). *Phys. Rev. Lett.*, **91**, 193201.
Sengupta, P., Pryadko, L. P., Alet, F., Troyer, M., and Schmid, G. (2005). *Phys. Rev. Lett.*, **94**, 207202.
Shih, M.-F., Segev, M., and Salamo, G. (1997). *Phys. Rev. Lett.*, **78**, 2551–2554.
Shlyapnikov, G. V. and Pedri, P. (2006). Conference on Many-Body Phenomena in Dipolar Systems (Dresden).
Strecker, K. E., Partridge, G. B., G., Truscott A., and Hulet, R. G. (2002). *Nature*, **417**, 150.
Stuhler, J., Griesmaier, A., Koch, T., Fattori, M., Pfau, T., Giovanazzi, S., Pedri, P., and Santos, L. (2005). *Phys. Rev. Lett.*, **95**, 150406.
Tikhonenkov, I., Malomed, B. A., and Vardi, A. (2008). *Phys. Rev. Lett.*, **100**, 090406.
Trefzger, C., Menotti, C., and Lewenstein, M. (2009). *Phys. Rev. Lett.*, **103**, 035304.
Vengalattore, M., Leslie, S. R., Guzman, J., and Stamper-Kurn, D. M. (2008). *Phys. Rev. Lett.*, **100**, 170403.
Wang, D. W. (2007). *Phys. Rev. Lett.*, **98**, 060403.
Wang, D. W. (2010). unpublished.
Wang, D. W. and Demler, E (2010). arXiv:0812.1838.
Wang, D.-W., Lukin, M. D., and Demler, E. (2006). *Phys. Rev. Lett.*, **97**, 180413.
Yi, S. and You, L. (2001). *Phys. Rev. A*, **63**, 053607.
Zakharov, V. E. and Shabat, A. B. (1972). *JETP*, **61**, 118.